A Study of the Coarsening in Tin/Lead Solders

W. Dreyer
Weierstraß Institut für Angewandte Analysis und Stochastik
Mohrenstraße 39
10117 Berlin
Germany

W. H. Müller
Department of Mechanical and Chemical Engineering
Heriot-Watt University, Riccarton
Edinburgh EH14 4AS
Great Britain

Abstract

This paper presents a model, which is capable to simulate the coarsening process observed during thermo-mechanical treatment of binary tin-lead solders. Fourier transforms and spectral theory are used for the numerical treatment of the thermo-elastic as well as of the diffusion problem encountered during phase separation in these alloys. More specifically, the analysis is based exclusively on continuum theory, first, relies on the numerical computation of the local stresses and strains in a representative volume element (RVE). Second, this information is used in an extended diffusion equation to predict the local concentrations of the constituents of the solder. Besides the classical driving forces for phase separation, as introduced by Fick and Cahn-Hilliard, this equation contains an additional term which links the mechanical to the thermodynamical problem. It connects internal and external stresses, strains, temperature, as well as concentrations and allows for a comprehensive study of the coarsening and aging process.

1 Introduction

Joining methods are critical for the reliable use of electronic packages. In particular, since the advent of surface mount technology (SMT) the reliability and lifetime of solder joints has been one of the paramount topics in the field of modern microelectronic packaging technology: Lau and Rice, 1985. The first two pictures in Figure 1 show a cross-sectional cut through the solder joint[1] of a micro-resistor, before and after thermal cycling between $-55°C$ and $+125°C$ according to military specification Mil-Std-883, method 1011. The third picture presents a cross-sectional cut through a solder ball of another microelectronic application, a ball grid array (BGA), after several thousand so-called power cycles. In this particular case the microelectronic chip in the BGA serves as a heat source and leads to accelerated aging of the solder as follows.

The regions of different shades of grey and black in the various solder joints indicate that the originally fine mix between tin (Sn) and lead (Pb) is superseded by "island formation" of high lead and tin concentrations. These form as a result of the separation of both phases, an aging process which is known as "coarsening" (Ozmat, 1990, p. 959, Harris *et al.*, 1991, p. 20, Pao, 1992, p. 559). More specifically, coarsening in SnPb solders must be attributed to the combined effect of three mechanisms.

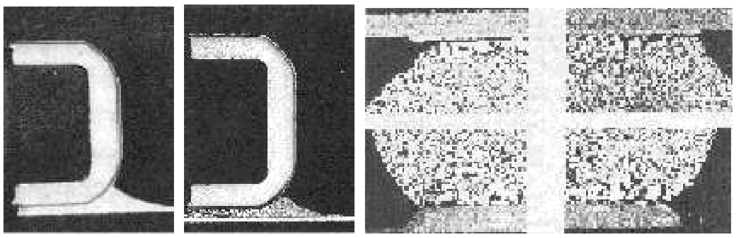

Fig. 1. Aging of SnPb solder joints used in SMT (Jendrny *et al.*, 1997, Albrecht and Gamalski, 1996).

The first mechanism is classical diffusion which initiates the process of coarsening and which can be described mathematically by Fick's law (see, e.g., Rothman, 1984, pp. 3). This process is particularly active at temperatures beyond 0.5 of the homologous temperature of the solder which explains the effectiveness of accelerated aging tests, such

[1] All joints shown are made of eutectic tin lead solder.

as the aforementioned power-cycling. In fact, finite element studies have shown (Hauck *et al.*, 1996) that power cycling can lead to local temperatures in the solder balls which are in the order of 150°C and more which corresponds to homologous temperatures greater than 0.8 .[2]

The second mechanism is surface tension which controls the number, steepness, orientation, and the final shape of the interfaces within the coarsened structure. Mathematically speaking, this effect can be assessed by an additional term in the diffusional flux which was originally suggested by Cahn and Hilliard (1958). For the outcome of the final microstructure it is important to note that the size of the surface tensions varies by several order of magnitudes depending on whether the interfaces are coherent, semicoherent, or incoherent (Ragavan and Cohen, 1975, pp. 77). Moreover, the size of the surface tensions is also influenced by temperature and, as it was emphasized before by Cahn and Hilliard (1958), p. 259, it can vary in the different directions of the crystal lattice. The latter will explain the typical eutectic structure observed in SnPb solders.

Third, thermo-mechanical stresses will also lead and enforce coarsening of a tin-lead microstructure (Seyyedi *et al.*, 1991, p. 51, Hacke *et al.*, 1997, p. 781, Nylen, 1997, p. 890). Their contribution to the diffusional flux is based on eigenstrains, which, locally, are due to the different thermal expansion lattice parameters of the anisotropic phases, and, globally, to the mismatch of the various materials involved in a microelectronics structure.

Consequently, as a result of the coarsening process the overall material properties of the solder must change over time. This will eventually have a detrimental effect on the mechanical stability of the joint. For example: The creep behavior of a solder is directly linked to grain size (Darveaux *et al.*, 1995, pp. 397, Hacke *et al.*, 1991), and the process of phase separation will lead to a decrease of the flow stress (Seyyedi *et al.*, 1997, p. 51). The micro-morphology of the solder will also influence the crack path during the fracture process (Logston *et al.*, 1990, pp. 205). Moreover, for near-eutectic SnPb solder bumps, which are attached to an interposer through several pads made of copper and/or nickel, localized coarsening is accompanied by the formation of intermetallics in the highly stressed interfacial areas which precedes cracking (see the interface regions in the micrographs of Figure 1, and Hwang and Lucey, 1993, p. 663, Flanders *et al.*, 1997).

From a technological point of view it is important to identify the factors that result in coarsening in solders. Once they are known and quantified it can be determined how to minimize their influence in order to increase the lifetime and the reliability of a solder joint and, hence, the electronic component. Eventually it may also become possible to change these properties by suitable doping agents or external stress conditions such that healing of the solder material is initiated. However, in order to identify the factors quantitatively a realistic model, based on continuum theory, needs to be developed first. The development of this model and first *qualitative* simulations of the coarsening phenomenon with realistic material data for SnPb solders are the prime objectives of this paper.

However, in a second step, experiments must be carried out which allow the measurement of material parameters to be used during *quantitative* numerical simulations. The development of such an analytically *and* experimentally correlated simulation tool for the quantitative description of coarsening in a binary alloy is the long-term goal of the authors.

[2]The homologous temperature is defined as the ratio between the current temperature and the melting temperature of the alloy, i.e., 180°C in the case of a eutectic SnPb solder.

2 The mathematical model

2.1 Assumptions and objectives

Consider a body, B , which consists of a binary alloy of lead (Pb) and tin (Sn) at a eutectic composition[3] (see the phase diagram shown in Figure 2). This body is divided into representative volume elements (RVEs) which are characterized by material coordinates $\underline{x} = (x_1, x_2, x_3)$ in space. In order to avoid additional complications the size of the RVE is such that it lies within one grain and grain boundaries need not to be modeled. Within the RVE there are regions of two different phases, the α-phase which is rich in lead, and the β-phase which is rich in tin (cp., Figure 2). The α-phase has cubic material symmetry and the β-phase has tetragonal symmetry (i.e., the symmetry of their dominant elements, lead and tin, respectively).

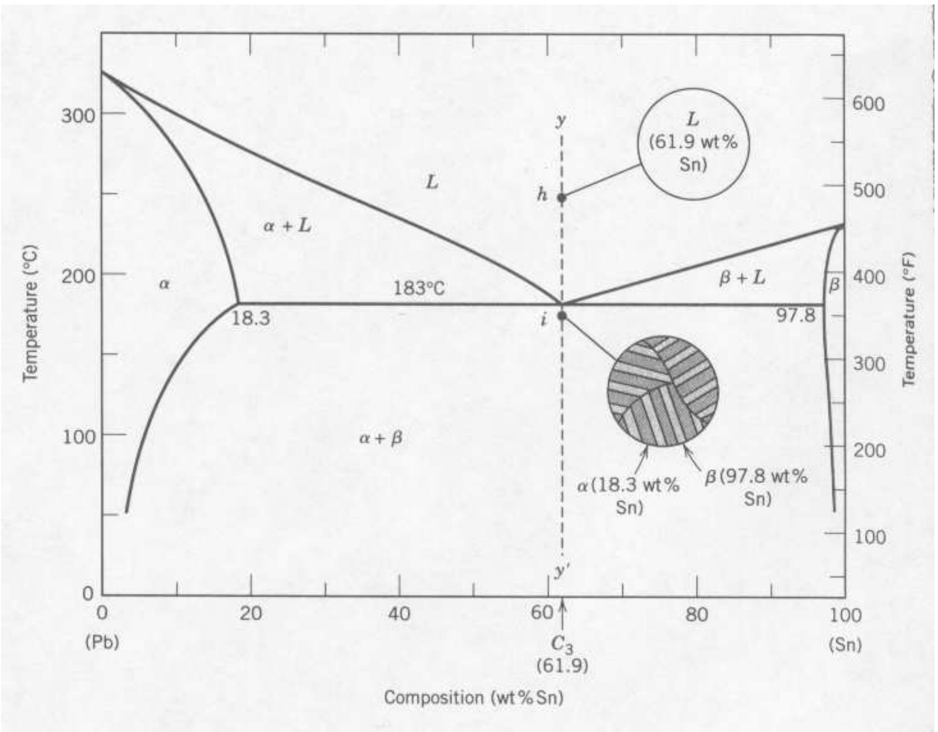

Fig. 2. The phase diagram of the binary alloy SnPb according to Callister (1997).

From the mathematical point of view, the final objective of the model is to determine the strain fields, $\varepsilon_{ij}(\underline{x}, t)$, and the field of the concentration of the tin, $c(\underline{x}, t) = c_{\mathrm{Sn}}(\underline{x}, t)$, for all points, $\underline{x} \in B$, and at all times, t. Moreover, for a binary mixture only one concentration field needs to be determined since, due to mass conservation, the following identity holds:

$$c_{\mathrm{Sn}}(\underline{x}, t) + c_{\mathrm{Pb}}(\underline{x}, t) = 1. \tag{2.1}$$

2.2 The mechanical aspects of the model

It will be assumed that mechanical equilibrium is much faster achieved than thermodynamical (or chemical) equilibrium. Consequently, the mechanical part of the problem

[3]For simplicity this paper concentrates on the eutectic compposition and the model will be geared toward the modeling of the eutectic microstructure.

or, in other words, the solution for the strain fields is based on the equation for static equilibrium of forces, i.e.:

$$\frac{\partial \sigma_{ij}}{\partial x_j} = 0, \tag{2.2}$$

where the symbol σ_{ij} denotes the stress tensor. In addition to these equations kinematic conditions and Hooke's law will be taken into account:

$$\varepsilon_{kl} = \frac{1}{2}\left(\frac{\partial u_k}{\partial x_l} + \frac{\partial u_l}{\partial x_k}\right), \qquad \sigma_{ij} = C_{ijkl}\left(\varepsilon_{kl} - \varepsilon^*_{kl}\right), \tag{2.3}$$

where ε_{kl} denotes the local total strains and u is the displacement field. ε^*_{kl} are the "eigenstrains" (i.e., nonelastic strains, such as thermal expansion, phase transformation, etc.; see Mura, 1987), and C_{ijkl} is the stiffness matrix. Initially, when the SnPb-crystal develops from the melt, the eigenstrains originate as a consequence of the coherency of the different crystal lattices of the two phases. However, the simulation and study of the nucleation phase is left to future research. In this work we concentrate on the case of an already existing incoherent structure which will inevitably result since the lattice constants of the cubic α-phase and the tetragonal β-phase of SnPb solder are extremely different. Then the eigenstrains result from different thermal expansion of the two phases and, therefore, we put:

$$\varepsilon^*_{kl}(\underline{x},t) = \alpha_{kl}(\underline{x},t)\cdot(T - T_R), \alpha_{kl}(\underline{x},t) = \theta(\underline{x},t)\alpha^\alpha_{kl} + (1 - \Theta(\underline{x},t))\alpha^\beta_{kl}, \tag{2.4}$$

where T_R is the reference temperature of the stress-free state which, in the present case, was chosen to be the solidus temperature of the eutectic solder. The symbols α^α_{ij} and α^β_{ij} are tensors of thermal expansion coefficients of the cubic α and of the tetragonal β-phase, respectively:

$$\alpha^\alpha_{ij} = \begin{pmatrix} \alpha^\alpha & 0 & 0 \\ 0 & \alpha^\alpha & 0 \\ 0 & 0 & \alpha^\alpha \end{pmatrix}, \quad \alpha^\beta_{ij} = \begin{pmatrix} \alpha^\beta_1 & 0 & 0 \\ 0 & \alpha^\beta_1 & 0 \\ 0 & 0 & \alpha^\beta_3 \end{pmatrix}. \tag{2.5}$$

To a first order approximation the elements of these matrices are given by the thermal expansion coefficients of *pure* lead and tin. In order to account for higher order terms Vegard's law (see Massalski, 1965) or rules of mixtures could be used to relate them to the thermal expansion coefficients of the pure materials. However, in view of the uncertainty of the other material parameters involved in the model this will not be done in this paper.

The shape function, $\Theta(\underline{x},t)$, of eqn (2.4) is defined by:

$$\Theta(\underline{x},t) = \frac{c^\beta - c(\underline{x},t)}{c^\beta - c^\alpha} \Longrightarrow \Theta(\underline{x},t) = \begin{cases} 0 & \text{if} \quad \underline{x} \in \beta \\ 1 & \phantom{\text{if}} \quad \underline{x} \in \alpha \end{cases}, \tag{2.6}$$

where c^β and c^α are the equilibrium concentrations of the α and of the β-phase. For a given temperature the equilibrium concentrations are constants, and they can be read off from the phase diagram shown in Figure 2. Therefore, the eigenstrains are directly connected to the local (continuous) composition, $c(\underline{x},t)$, of the alloy. The shape function is also used to characterize the spatial dependence of other material parameters, such as the local stiffness:

$$C_{ijkl}(\underline{x},t) = \Theta(\underline{x},t)C^\alpha_{ijkl} + (1 - \Theta(\underline{x},t))C^\beta_{ijkl}. \tag{2.7}$$

the tensor of surface tensions:

$$a_{ij}(\underline{x},t) = \Theta(\underline{x},t)a_{ij}^{\alpha} + (1-\Theta(\underline{x},t))a_{ij}^{\beta}, \tag{2.8}$$

and the matrix of mobility coefficients:

$$M(\underline{x},t) = \Theta(\underline{x},t)M^{\alpha} + (1-\Theta(\underline{x},t))M^{\beta}. \tag{2.9}$$

The indices α and β in these equations refer to properties of the α and of the β-phase, respectively, which are assumed to be constant and known material quantities. Specifically, for the stiffness tensor, Voigt's coefficients, $C_{ij}^{\alpha/\beta}$, are preferably used in data handbooks. They are related to $C_{ijkl}^{\alpha/\beta}$ as follows:

$\begin{matrix} kl \\ ij \end{matrix}$	11	22	33	23	31	12
11	C_{11}^{α}	C_{12}^{α}	C_{12}^{α}	0	0	0
22	C_{12}^{α}	C_{11}^{α}	C_{12}^{α}	0	0	0
33	C_{12}^{α}	C_{12}^{α}	C_{11}^{α}	0	0	0
23	0	0	0	C_{44}^{α}	0	0
31	0	0	0	0	C_{44}^{α}	0
12	0	0	0	0	0	C_{44}^{α}

,

$\begin{matrix} kl \\ ij \end{matrix}$	11	22	33	23	31	12
11	C_{11}^{β}	C_{12}^{β}	C_{13}^{β}	0	0	0
22	C_{12}^{β}	C_{11}^{β}	C_{13}^{β}	0	0	0
33	C_{13}^{β}	C_{13}^{β}	C_{33}^{β}	0	0	0
23	0	0	0	C_{44}^{β}	0	0
31	0	0	0	0	C_{44}^{β}	0
12	0	0	0	0	0	C_{66}^{β}

. (2.10)

Initially a suitable function of position will be assumed for $c(\underline{x},t)$ (e.g., nuclei in form of localized tin-rich regions), which, by virtue of eqns (2.4-2.6), provides an initial condition for the eigenstrains ε_{kl}^{*}. The resulting stresses and strains will then be computed from eqns (2.2-2.3). In the next subsection it will be discussed how this can be achieved for the initial time as well as during the subsequent time steps.

2.3 Solution of the mechanical problem

Recently spectral methods or, more specifically, *discrete Fourier transforms* (DFT) have been used in an extremely promising way to solve stress/strain problems in heterogeneous solids (e.g., Canuto *et al.*,1988, Suquet, 1990, Moulinec and Suquet, 1994, 1998, Dreyer (1994), Dreyer *et al.*, 1998, Müller, 1996, 1998a / b, Müller and Neumann, 1998). Specifically we will consider the case that loads $\sigma_{xx}^{0}, \sigma_{xy}^{0}, \sigma_{yy}^{0}$ are specified along the periphery of the RVE (cf., Figure 3, left) are specified as follows:

$$\int\limits_{2\pi L} \sigma_{xx} dy + \int\limits_{2\pi L} \sigma_{xy} dy = \left(\sigma_{xx}^{0} + \sigma_{xy}^{0}\right) 2\pi L, \quad \int\limits_{2\pi L} \sigma_{yy} dx + \int\limits_{2\pi L} \sigma_{xy} dx = \left(\sigma_{yy}^{0} + \sigma_{xy}^{0}\right) 2\pi L, \tag{2.11}$$

where σ_{xy} follows from the solution of eqns (2.2-2.3). Following Müller (1998a) consider an array of N points, $\underline{x}$, in a physical space of dimension d, arranged equidistantly over a square unit cell lattice of length L, (see Fig. 3, right):

$$\underline{x} = h\underline{\alpha}, \underline{\alpha} = (\alpha_1, \ldots, \alpha_d), \quad \alpha_j \in \{0, 1, \ldots, N-1\}, \quad (j,d) \in \{1,2,3\}, \quad h = \frac{2\pi L}{N}. \tag{2.12}$$

Let discrete field variables, $f(\underline{\alpha})$, be defined in each of these points. Then the *discrete Fourier transform* for these variables can be obtained by summation:

$$\hat{f}(\underline{s}) = \frac{1}{N^{d/2}} \sum_{\alpha_1=0}^{N-1} \cdots \sum_{\alpha_d=0}^{N-1} f(\underline{\alpha}) \exp\left(i2\pi \frac{\underline{s}\cdot\underline{\alpha}}{N}\right) \equiv Y\left[f(\underline{\alpha})\right]. \tag{2.13}$$

If *periodicity conditions* hold across the representative volume element, RVE:

$$f(\underline{\alpha} + N\underline{r}) = f(\underline{\alpha}), \qquad \underline{r} = (r_1, \ldots, r_d), \qquad r_j \in Z \tag{2.14}$$

the corresponding quantities $f(\underline{\alpha})$ in physical space can be obtained through Fourier's theorem provided that $\hat{f}(\underline{s})$ is known:

$$f(\underline{\alpha}) = \frac{1}{(N)^{d/2}} \sum_{s_1=0}^{N-1} \cdots \sum_{s_d=0}^{N-1} \hat{f}(\underline{s}) \exp\left(-i\frac{2\pi}{N}\underline{s}\cdot\underline{\alpha}\right) \equiv Y^{-1}\left[\hat{f}_{(s)}\right]. \tag{2.15}$$

Note that all summations are *finite* and can be performed *exactly*, e.g., by fast Fourier transform. The sums do *not* represent an approximation of continuous Fourier integrals. As in the continuous case, a differentiation rule holds:

$$Y\left(\frac{\partial f(\underline{\alpha})}{\partial x_j}\right) = \xi_j(s_j) Y(f(\underline{\alpha})) + O(h^2), \xi_j(s_j) = -\frac{i}{h}\sin\left(\frac{h}{L}s_j\right). \tag{2.16}$$

This rule is an approximation of spatial differentiation by a central difference quotient and it is based on the *shift theorem* which requires the *periodicity conditions* (2.14) to hold. Second derivatives can be treated similarly:[4]

$$\begin{gathered} Y\left(\frac{\partial^2 f(\underline{\alpha})}{\partial x_j^2}\right) = \xi_{\underline{jj}}(s_j) Y(f(\underline{\alpha})) + O(h^2), \qquad \xi_{\underline{jj}}(s_j) = \frac{2}{h^2}\left(\cos\left(\frac{h}{L}s_j\right) - 1\right), \\ Y\left(\frac{\partial^2 f(\underline{\alpha})}{\partial x_i \partial x_j}\right) = \xi_{ij}(s_i, s_j) Y(f(\underline{\alpha})) + O(h^2), \quad \xi_{ij}(s_i, s_j) = -\frac{1}{h^2}\sin\left(\frac{h}{L}s_i\right)\sin\left(\frac{h}{L}s_j\right), i \neq j. \end{gathered} \tag{2.17}$$

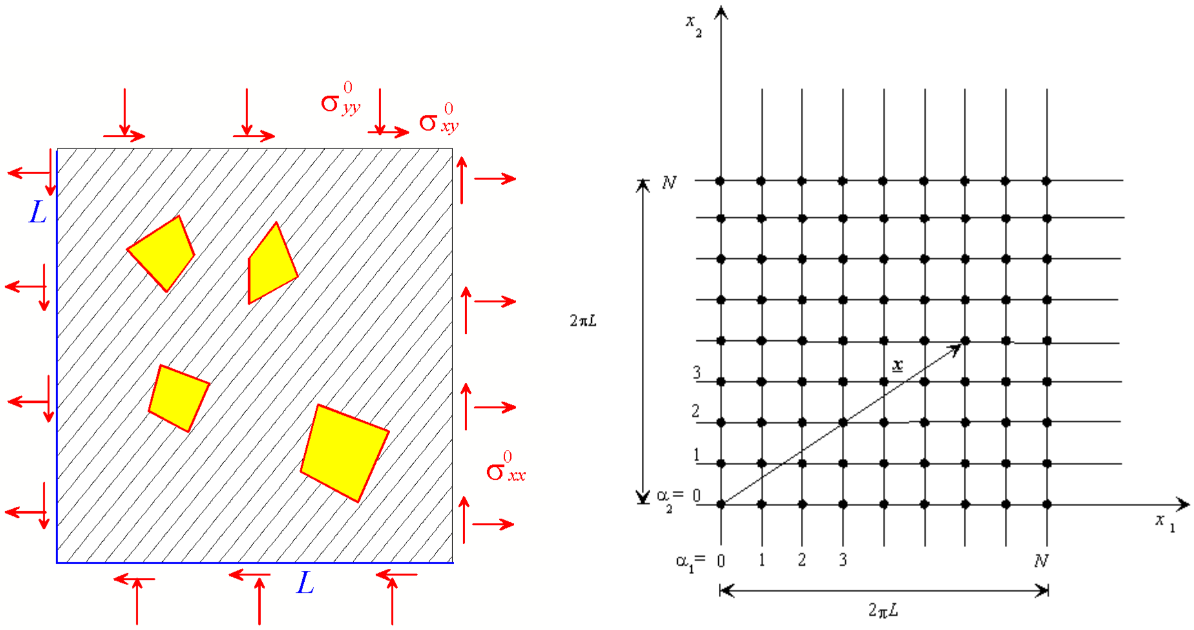

Fig. 3. Square RVE and its discretization in the two-dimensional case, $N = 8$.

DFT will now be applied to eqns (2.1), (2.2), i.e., to static, linear-elastic problems with small deformations and to solve the resulting PDE of second order. To this end we make use of the equivalent inclusion technique (EIT) which goes back to Eshelby (Mura, 1987).

[4]Some of the indices are underlined in order to indicate that no summation is implied.

This method circumvents the problem of the spatial dependence of the stiffness matrix by introducing an auxiliary strain field $\varepsilon^H_{kl}(\underline{\alpha})$ (Moulinec and Suquet, 1998, and Müller, 1998a) and an auxiliary constant stiffness matrix, C^H_{ijkl}, as follows:

$$\sigma_{ij}(\underline{\alpha},t) = C_{ijkl}(\underline{\alpha},t)\left(\varepsilon_{kl}(\underline{\alpha},t) - \varepsilon^*_{kl}(\underline{\alpha},t)\right) = C^H_{ijkl}\left(\varepsilon_{kl}(\underline{\alpha},t) - \varepsilon^*_{kl}(\underline{\alpha},t) - \varepsilon^H_{kl}(\underline{\alpha},t)\right). \tag{2.18}$$

If this is inserted into eqns (2.2) an (2.3) the following problem remains to be solved:

$$C^H_{ijkl}\frac{\partial^2}{\partial x_j \partial x_l}u_k = c^H_{ijkl}\frac{\partial}{\partial x_j}\left(\varepsilon^H_{kl} + \varepsilon^*_{kl}\right). \tag{2.19}$$

Periodicity of all fields is assumed and by virtue of the differentiation theorems (2.16) and (2.17) this system of PDEs is mapped onto a system of linear equations in Fourier space for which one formal solution can be obtained as follows:

$$\varepsilon_{kl}(\underline{\alpha},t) = Y^{-1}\left\lfloor \hat{A}^H_{klop}\hat{\varepsilon}^H_{op}\right\rfloor(\underline{\alpha},t) + Y^{-1}\left\lfloor \hat{A}^H_{klop}\hat{\varepsilon}^H_{op}\right\rfloor(\underline{\alpha},t), \tag{2.20}$$

where:

$$\hat{A}^H_{ijkl} = \begin{cases} & 0, \quad \underline{s} = \underline{0} \\ \frac{1}{2D}\left(\xi_i N_{js} + \xi_j N_{is}\right) C^H_{srkl}\xi_r, & \underline{s} \neq \underline{0} \end{cases}. \tag{2.21}$$

The symbols N_{js} and D are the discriminant and determinant of the following matrix:

$$M_{ik} = C^H_{ijkl}\xi_{jl} \Longrightarrow M^{-1}_{ik} = \frac{N_{ik}}{D} \tag{2.22}$$

They are cumbersome but known functions of the stiffness C^H_{ijkl} (which will soon be chosen suitably), and of the Fourier transforms of the difference quotients (2.17) which, for an arbitrary degree of anisotropy, are preferably determined by means of analytical software packages, such as Mathematica®. In particular, for the cubic phase, the following concise relations can be used directly:

$$\begin{aligned} D &= -\mu(\lambda + 2\mu + \mu')(\xi_{kk})^2 - (\lambda + \mu + \mu')^2\xi_{11}\xi_{22} + (\lambda+\mu)^2\xi_{12}^2, \\ N_{ij} &= -\lfloor(\lambda + 2\mu + \mu')\xi_{kk}\delta_{ij} - (\lambda+\mu)\xi_{ij} - \mu'\delta_{ijkl}\xi_{kl}\rfloor, \end{aligned} \tag{2.23}$$

where $\delta_{ij}, \delta_{ijkl}$, denote Kronecker symbols and λ, μ and μ' are Lamé's constants, respectively.

The choice $\hat{A}^H_{ijkl}(\underline{s} = \underline{0}) = 0$ implies that we currently consider the case of vanishing mean strains. In fact, mean strains are defined by:

$$\bar{\varepsilon}_{ij} = \frac{1}{N^d}\sum_{\alpha_1=0}^{N-1}\cdots\sum_{\alpha_d=0}^{N-1}\varepsilon_{ij}(\underline{\alpha}). \tag{2.24}$$

On the other hand the definition of Fourier transforms according to eqn (2.13) leads to:

$$\hat{\varepsilon}_{ij}(\underline{0}) = \frac{1}{(N)^{d/2}}\sum_{s_1=0}^{N-1}\cdots\sum_{s_d=0}^{N-1}\varepsilon_{ij}(\underline{\alpha}). \tag{2.25}$$

Mutual insertion of eqns (2.24) and (2.25) yields:

$$\bar{\varepsilon}_{ij} = \frac{1}{(N)^{d/2}}\hat{\varepsilon}_{ij}(\underline{0}), \tag{2.26}$$

and since (cf., eqns (2.20) and (2.21)):

$$\hat{\varepsilon}_{ij}(\underline{0}) = \hat{A}^H_{ijkl}(\underline{0})\hat{\varepsilon}^H_{kl}(\underline{0}) + \hat{A}^H_{ijkl}(\underline{0})\hat{\varepsilon}^*_{kl} = 0 \cdot \hat{\varepsilon}^H_{kl}(\underline{0}) + 0 \cdot \hat{\varepsilon}^*_{kl}(\underline{0}) = 0, \tag{2.27}$$

it finally follows that:

$$\bar{\varepsilon}_{ij} = 0. \tag{2.28}$$

The solution shown in eqns (2.20) and (2.21) solves the original PDE, however, it does not take the boundary condition (2.11) into account yet. Before we start to generalize this solution appropriately it is necessary to eliminate the auxiliary field $\hat{\varepsilon}^H_{op}$. To this end we insert eqns (2.15) and (2.20) into (2.18) to obtain:

$$\begin{aligned} &C^H_{ijkl}\left(Y^{-1}\left[\hat{A}^H_{klop}\hat{\varepsilon}^H_{op}\right](\underline{\alpha},t) + Y^{-1}\left[\hat{A}^H_{klop}\hat{\varepsilon}^H_{op}\right](\underline{\alpha},t) - \varepsilon^*_{kl}(\underline{\alpha},t) - \varepsilon^H_{kl}(\underline{\alpha},t)\right) = \\ &\left(C^\beta_{ijkl} - \Theta(\underline{\alpha},t)\left[C^\beta_{ijkl} - C^\alpha_{ijkl}\right]\right)\left(Y^{-1}\left[\hat{A}^H_{klop}\hat{\varepsilon}^H_{op}\right](\underline{\alpha},t) + Y^{-1}\left[\hat{A}^H_{klop}\hat{\varepsilon}^*_{op}\right](\underline{\alpha},t) - \varepsilon^*_{kl}(\underline{\alpha},t)\right). \end{aligned} \tag{2.29}$$

In what follows the "growth" of the softer α-phase in an initially uniform β-matrix will be studied. Then, in order to guarantee convergence, the constant C^H_{ijkl} matrix should be chosen as (cf., Müller, 1998a):

$$C^H_{ijkl} = C^\beta_{ijkl} \tag{2.30}$$

which results in:

$$C^\beta_{ijkl}\varepsilon^H_{kl}(\underline{\alpha},t) = \Theta(\underline{\alpha},t)\left(C^\beta_{ijkl} - C^\alpha_{ijkl}\right)\left(Y^{-1}\left[\hat{A}^\beta_{klop}\hat{\varepsilon}^H_{op}\right](\underline{\alpha},t) + Y^{-1}\left[\hat{A}^\beta_{klop}\hat{\varepsilon}^*_{op}\right](\underline{\alpha},t) - \varepsilon^*_{kl}(\underline{\alpha},t)\right). \tag{2.31}$$

This is a functional equation for the unknown field $\varepsilon^H_{kl}(\underline{\alpha},t)$ which is solved in the standard Neumann fashion:

$$\begin{aligned} &\overset{(n+1)}{\varepsilon}{}^H_{kl}(\underline{\alpha},t) = \\ &\Theta(\underline{\alpha},t)(C^\beta)^{-1}_{klrs}(C^\beta_{rsmn} - C^\alpha_{rsmn})\left(Y^{-1}\left[\hat{A}^\beta_{mnop}\overset{(n)}{\hat{\varepsilon}}{}^H_{kl}\right](\underline{\alpha},t) + Y^{-1}\left[\hat{A}^\beta_{mnop}\hat{\varepsilon}^*_{op}\right](\underline{\alpha},t) - \varepsilon^*_{mn}(\underline{\alpha},t)\right), \end{aligned} \tag{2.32}$$

where the 0-th iteration strain field is given by the strain of a homogeneous RVE subjected to exter-nal loads (see Figure 3):

$$\overset{(0)}{\varepsilon}{}^H_{kl} = \left(C^\beta\right)^{-1}_{ijkl}\sigma^0_{kl}. \tag{2.33}$$

Y^{-1} denotes the inverse discrete Fourier transform defined in eqn (2.13) and (2.14) and the symbols $\hat{A}^\beta_{mnop}$ can be computed from $\hat{A}^H_{mnop}$ (see eqn (2.21)) if C^H_{ijkl} is substituted by C^β_{ijkl}. In fact, EIT was originally developed for the continuum and eqn (2.32) is the discrete counterpart of the Neumann iteration technique for the solution of a Fredholm integral equation for the continuous field $\varepsilon^H_{kl}(\underline{x})$. For completeness, it should be pointed out that in the present situation, for a given external net stress σ^0_{ij}, eqn (2.33) for the 0-th order strain field is also evaluated by using C^β_{ijkl}.

It should be noted that the relations for the thermal expansion coefficients, the stiffness tensor, the surface tensions, and for the mobility tensor shown in eqns (2.5) and (2.6)-(2.9) maintain their simple form only if the coordinate systems of the RVE, x_i, and of the crystallographic axes of the phases, x'_j, coincide. However, this will be the exception and in most cases both coordinate systems are linked to each other by a transformation matrix, $O_{ij}^{\alpha/\beta}$,[5] which is different from unity:

$$x_i = O_{ij}^{\alpha/\beta} x'_j. \tag{2.34}$$

Consequently:

$$\alpha_{ij}^{\alpha/\beta} = O_{ir}^{\alpha/\beta} O_{js}^{\alpha/\beta} \alpha'^{\alpha/\beta}_{rs}, \tag{2.35}$$

and:

$$C_{ijkl}^{\alpha/\beta} = O_{ir}^{\alpha/\beta} O_{js}^{\alpha/\beta} O_{kt}^{\alpha/\beta} O_{lu}^{\alpha/\beta} C'^{\alpha/\beta}_{rstu}, \tag{2.36}$$

where the matrices $C'^{\alpha/\beta}_{rstu}$ and $\alpha'^{\alpha/\beta}_{rs}$ have the form as indicated before in eqns (2.10) and (2.5), respectively. Eqns (2.35) and (2.36) can now be used to compute the local eigenstrains and stiffnesses according to eqns (2.4) and (2.7), as well as the symbols $\hat{A}_{mnop}^{\alpha/\beta}$ according to eqns (2.21) and (2.22). It should be pointed out that symbolic computation of these symbols is extremely tedious, especially for tetragonal symmetry. In fact, this became only feasible by using various features of the Mathematica® software package to create a reliable FORTRAN file.

To summarize this subsection it seems worth recalling that loading of the body is taken into account in two ways: First, it can be due to internal eigenstrains, ε_{kl}^*. In the present case these will evolve as a consequence of the different thermal expansion coefficients of the tin and of the lead rich phase.

Second, loading can be also imposed from outside by prescribing suitable mean averages for the stresses, σ_{ij}^0, along the boundary of the RVE: (see eqns (2.11) and (2.33)). Physically speaking, these are due to the global thermal mismatch of the microelectronic structure and/or to direct mechanical straining of the solder, e.g., by shear testing (see Nylén *et al.*, 1997, p. 891).

2.4 The thermodynamical aspects of the model

Once the local stresses and strains are known at a certain time, t, they will be used to compute the evolvement of the distribution of concentrations, c, of during the next time-step, Δt. This follows from a numerical solution of the diffusion equation:

$$\frac{\partial c}{\partial t} + \frac{\partial J_i}{\partial x_i} = 0, \tag{2.37}$$

with the following extended diffusion flux, J_i:

$$J_i = -M \frac{\partial}{\partial x_i} \left(\frac{\partial \Psi}{\partial c} - a_{kl} \frac{\partial^2 c}{\partial x_k \partial x_l} + \frac{\partial}{\partial c} \left[\frac{1}{2} (\varepsilon_{ij} - \varepsilon_{ij}^*) C_{ijkl} (\varepsilon_{kl} - \varepsilon_{kl}^*) \right] \right), \tag{2.38}$$

where M is the (scalar) mobility factor which will be related to the mobility of the α and of the β-phase as shown in eqn (2.9).

Moreover, Ψ is the configurational part of the Gibbs' free energy density of the system, which will be assumed in form of a suitable Landau polynomial (see below). A sketch of the derivation of eqns (2.37) and (2.38) is presented in Appendix A.

[5] The suffix α/β indicates that both phases could still be oriented differently

Note that the first term in the diffusion flux leads to the classical diffusion equation as proposed by Fick (e.g., Rothman, 1984, pp. 3), whereas the second part contains extensions of the diffusion equation as introduced by Cahn and Hilliard, α_{ij} being the matrix of surface tension related quantities (see Cahn and Hilliard, 1958, and de Fontaine, 1975, or Hawick, 1991, Chapter 3, for a comprehensive summation of the original results which is related to the surface tension coefficients of the α and of the β-phase as shown in eqn (2.8)).

Note that the diffusional flux shown in eqn (2.38) contains an additional term which characterize the influence of mechanical stresses on the diffusion process *explicitly*:

$$\frac{\partial}{\partial c}\left(\frac{1}{2}\left(\varepsilon_{ij}-\varepsilon^*_{ij}\right)C_{ijkl}\left(\varepsilon_{kl}-\varepsilon^*_{kl}\right)\right)=-\sigma_{kl}\frac{\partial\varepsilon^*_{kl}}{\partial c}+\frac{1}{2}\left(\varepsilon_{ij}-\varepsilon^*_{ij}\right)\frac{\partial C_{ijkl}}{\partial c}\left(\varepsilon_{kl}-\varepsilon^*_{kl}\right). \quad (2.39)$$

As a result, the computed change in concentrations during the time Δt will lead to a change of the micromorphology and, consequently, necessitates an update of the local stress/strain distribution in the RVE by means of eqns (2.32), (2.33). If this has been achieved, the next time-step can be considered, etc. Some details of the numerical procedures involved will be presented in the next subsection.

In order to guarantee coexistence of both phases α and β the density of the Gibbs' free energy needs to be a non-convex function of the concentrations, for example (see Cahn and Hilliard, 1958, p. 261, or Tsakalalos, 185, p. 150):

$$\Psi=\Psi_0\left(\left([c^\alpha-c_0]^2-[c-c_0]^2\right)^2-b[c-c_0]\right),\qquad c_0=\frac{1}{2}(c^\alpha+c^\beta) \quad (2.40)$$

where Ψ_0 and b are temperature dependent coefficients which need to be adjusted suitably (see Subsection 3.1), and c^α, c^β are the equilibrium concentrations which were mentioned in Subsection 2.4.

2.5 Some remarks on the numerical treatment of the extended diffusion equation

The extended diffusion equation (2.37) and (2.38) is mapped into discrete Fourier space and the Fourier transforms of spatial differential quotients are replaced according to eqns (2.17):

$$\frac{1}{M}\frac{d\hat{c}}{dt}=\xi_{ii}Y\left(\frac{\partial\Psi}{\partial c}\right)-\hat{a}_{kl}\xi_{ii}\xi_{kl}\hat{c}-\xi_{ii}Y\left(\frac{\partial}{\partial c}\left[\frac{1}{2}(\varepsilon_{ij}-\varepsilon^*_{ij})C_{ijkl}(\varepsilon_{kl}-\varepsilon^*_{kl})\right]\right). \quad (2.41)$$

To this end it was assumed that:

$$M^\alpha=M^\beta=M. \quad (2.42)$$

This was done mainly in view of the missing data regarding the mobility and diffusivity coefficients of both species. It is left to future research to make use of the additional possibilities eqn (2.9) has to offer. A dimensionless time is introduced:

$$\tilde{t}=t\frac{M\Psi_0}{L^2}=n\Delta\tilde{t},\qquad n\in N. \quad (2.43)$$

The time derivative is approximated in the usual manner, and an implicit scheme is used for its integration:

$$\begin{aligned}\frac{\hat{c}^{n+1}-\hat{c}^n}{\Delta\tilde{t}} &= \tilde{\xi}_{ii}Y\left(\frac{\partial\tilde{\Psi}}{\partial c}\right)\bigg|_{\hat{c}=\hat{c}^n} - \tilde{\alpha}^{\beta}_{kl}\tilde{\xi}_{ii}\tilde{\xi}_{kl}\hat{c}^{n+1} + (\tilde{\alpha}^{\beta}_{kl}-\tilde{\alpha}^{\alpha}_{kl})\tilde{\xi}_{ii}Y\left(\frac{\partial^2\Theta c}{\partial\tilde{x}_k\partial\tilde{x}_l}\right)\bigg|_{\hat{c}=\hat{c}^n} - \\ & \xi_{ii}Y\left(\tilde{\sigma}_{kl}\frac{\partial\varepsilon^*_{kl}}{\partial c}\right)\bigg|_{\hat{c}=\hat{c}^n} + \xi_{ii}Y\left(\frac{1}{2}(\varepsilon_{ij}-\varepsilon^*_{ij})\frac{\partial\tilde{C}_{ijkl}}{\partial c}(\varepsilon_{kl}-\varepsilon^*_{kl})\right)\bigg|_{\hat{c}=\hat{c}^n},\end{aligned} \tag{2.44}$$

with dimensionless quantities:

$$\tilde{\xi}_{\underline{jj}}(s_j)=2\left(\frac{N}{2\pi}\right)^2\left(\cos\left(\frac{2\pi}{N}s_j\right)-1\right), \tilde{\xi}_{ij}(s_i,s_j)=-\left(\frac{N}{2\pi}\right)^2\sin\left(\frac{2\pi}{N}s_i\right)\sin\left(\frac{2\pi}{N}s_j\right),\ i\neq j, \tag{2.45}$$

$$\tilde{\Psi}=\frac{\Psi}{\Psi_0},\quad \tilde{\tilde{\alpha}}_{kl}=\frac{\alpha_{kl}}{\Psi_0 L^2},\quad \tilde{\sigma}_{kl}=\frac{\sigma_{kl}}{c},\quad \tilde{C}_{ijkl}=\frac{C_{ijkl}}{\Psi_0},\quad \tilde{x}_l=\frac{x_l}{L}. \tag{2.46}$$

2.6 A brief comparison with the literature

DFT techniques have been used before to solve extended diffusion equations, such as (2.37) and (2.38). Particularly noteworthy is the work of the school headed by Khachaturyan (see, e.g., Khachaturyan *et al.*, 1995, Chen *et al.*, 1991, McCormack *et al.*, 1992, Wang *et al.*, 1991, 1993a, 1993b, 1994, Wang and Khachaturyan, 1995, 1997), the papers of Nishimori and Onuki (1990), Li and Chen (1997), and Laberge *et al.* (1997), and the work by Koyama, Miyazaki and co-authors (e.g., Takeuchi *et al.*, 1990, Miyazaki *et al.*, 1991, Koyama *et al.*, 1994, 1996, Koyama and Miyazaki, 1994, 1998, Mebed *et al.*, 1997, Miyazaki and Koyama, 1996, 1997).

Even though there is a certain resemblance between the solution procedures used therein and the one outlined in Subsection 2.5 there are also fundamental differences, as follows:

- The physical concepts presented in the aforementioned papers are *not* based on the concepts of continuum theory alone. Rather they rely heavily on a microscopic formalism, also referred to as the stochastic field approach, which requires the use of kinetic coefficients together with atomic interaction energies, and fluctuation potentials.

- A complete continuum mechanics solution for the stress and strain fields, i.e., of eqns (2.2) and (2.3) is *not* performed. Rather the influence of the mechanical stresses and strains are taken into account indirectly. To this end the local elastic strain energy density is used (e.g., Li and Chen, 1997, eqn (3), Koyama and Miyazaki, 1998, eqn (22)) which is then evaluated by means of the Green's function solution shown in eqns (2.20) and (2.21). In there an average stiffness C^0_{ijkl} is inserted which, as it was pointed out by Li and Chen (1997), p. 1273, is an effective medium *approximation* which is legitimate provided the differences of the stiffnesses between the various phases are not too large. However, in the present case such an assumption seems questionable since the ratio of Young's moduli for (polycrystalline) tin and lead is roughly 3 : 1 (cf., Winter, 1998), and an iterative solution as shown in eqns (2.32) and (2.33) seems more appropriate.

- In the recent work by Koyama and Mizaki (1998, eqn (23)), the local variation in stiffness is accounted for very similarly to eqn (2.7). The only difference is the use of another shape function as the one shown in eqn (2.6). If this difference is taken into account, and if one specializes to cubic symmetry the two mechanical contributions to the diffusion flux in eqn (2.38) and (2.39) are identical with their expression for the strain energy contribution to the chemical potential, μ_{str}, eqn (26). However, the expression for the mobility as suggested by Koyama and Miyazaki in their eqn (7), is clearly different from the one shown eqn (2.9). For lack of data it is difficult to say how this difference influences the development of the microstructure. As it was mentioned before this aspect is left to future research.

- Simulations with materials that show a higher degree of anisotropy than cubic symmetry have not been reported by the aforementioned authors. As indicated before, some of their equations hold for cubic materials only. Also, no attempt was made to study the case where the axes of the RVE or, in other words, the orientation of the externally applied forces and the main crystallographic axes do not coincide.

3 Results and discussion

3.1 Choice of material constants

The thermal expansion coefficients and the elasticity constants of the lead and of the tin rich phase were approximated by the corresponding data for the pure elements (Lee and Raynor, 1954, p. 739, Handbook of Chemistry and Physics, 1995, p. 12-38, 12-40, 12-172):

$$\begin{aligned}
\alpha^\alpha &= 28.9\cdot 10^{-6}K^{-1},\ \alpha_1^\beta = 16.7\cdot 10^{-6}K^{-1},\ \alpha_3^\beta = 36.4\cdot 10^{-6}K^{-1}, && (3.1)\\
C_{11}^\alpha &= 49.66\text{GPa},\quad C_{12}^\alpha = 42.31\text{GPa},\quad C_{44}^\alpha = 14.98\text{GPa}, && (3.2)\\
C_{11}^\beta &= 75.29\text{GPa},\quad C_{12}^\beta = 61.56\text{GPa},\quad C_{13}^\beta = 44.00\text{GPa}, && \\
C_{33}^\beta &= 95.52\text{GPa},\quad C_{44}^\beta = 21.93\text{GPa},\quad C_{66}^\beta = 23.36\text{GPa}, && (3.3)
\end{aligned}$$

The equilibrium concentrations of the α and of the β-phase, c^α and c^β, can be read off from the phase diagram shown in Figure 2. Note that they are not symmetrically arranged in the following sense:

$$c^\alpha \neq 1 - c^\beta. \tag{3.4}$$

Indeed, if the temperature of the eutectic is increased from $-40°$C to the melting temperature at $+183°$C, the concentration c^α shows a considerable variation between 1% and 18,3%, whereas c^β changes by less than 3%. Two considerably different temperature levels have been selected:

$$\begin{aligned}
T_{\text{high}} &= 150°\text{C}:\quad c^\alpha = 11.88\%,\quad c^\beta = 97.98\%, && (3.5)\\
T_{\text{low}} &= 20°\text{C}:\quad c^\alpha = 1.54\%,\quad c^\beta = 99.86\%. && (3.6)
\end{aligned}$$

Note that if the ordinary Maxwell or common tangent construction (Raynor, pp. 293) is applied to the quadric chosen for the Gibbs' free energy in eqn (2.37) the following result is obtained:

$$\left.\frac{\partial\Psi}{\partial c}\right|_{c=c^\alpha} = -\Psi_0 b,\ \left.\frac{\partial\Psi}{\partial c}\right|_{c=c^\beta} = -\Psi_0 b,\ \frac{\Psi(c^\beta)-\Psi(c^\alpha)}{c^\beta - c^\alpha} = -\Psi_0 b, \tag{3.7}$$

which is independent of the choice of c^α and c^β. In fact the remaining factor, b, is irrelevant for the temporal evolution of the concentration profile (cf., eqns (2.37/2.38)) and, therefore, it is unnecessary to give it a value.

Reliable data for the various surface tension related quantities, a_{ij}^α and a_{ij}^β, of eqn (2.8) is difficult to obtain. They will depend on the crystallographic direction just as the surface tensions in single crystals do (cf., Sundquist, 1964). To the best knowledge of the authors no data for the surface tensions of pure lead and tin single crystals is available. Nevertheless, the following statements can be made:

- Due to the dominance of the lead the α-phase is cubic, and (cf. Cahn and Hilliard, p. 259) the matrix a_{ij}^α will be isotropic:

$$a_{ij}^\alpha = a^\alpha \delta_{ij}. \tag{3.8}$$

- Similarly, for the tetragonal β-phase, the matrix a_{ij}^β must be diagonal with respect to the main crystallographic axes:

$$a_{ij}^\beta = \begin{pmatrix} a_1^\beta & 0 & 0 \\ 0 & a_1^\beta & 0 \\ 0 & 0 & a_3^\beta \end{pmatrix}_{ij} . \tag{3.9}$$

- The crystal lattice parameters for pure lead and pure tin are given by (Winter, 1998):

$$r_1^{\mathrm{Pb}} = r_2^{\mathrm{Pb}} = r_3^{\mathrm{Pb}} = 495.08pm,\ r_1^{\mathrm{Sn}} = r_2^{\mathrm{Sn}} = 583.18pm,\ r_3^{\mathrm{Sn}} = 318.19pm. \tag{3.10}$$

They depend on the temperature, and for a first order approximation they can also be used to characterize the lattice parameters of the α and of the β-phase.[6] These parameters can now be used to rank the coefficients, $a^\alpha, a_1^\beta, a_3^\beta$, with respect to each other. For that purpose arguments similar to Cahn and Hilliard (1958), pp. 262 are used to, first, arrive at the following formulae:

$$a^\alpha = \frac{1}{3}\sum_n Z_n r_n^2 \nu_n,\ a_1^\beta = \frac{1}{2}\sum_n \left(Z_n - \sum_{\alpha=1}^{Z_n} \cos^2(\vartheta^\alpha)\right) r_n^2 \nu_n,\ a_3^\beta = \sum_n \left(\sum_{\alpha=1}^{Z_n} \cos^2(\vartheta^\alpha)\right) r_n^2 \nu_n, \tag{3.11}$$

where n identifies the coordination shell at a radius r_n from a center point atom, Z_n denotes the coordination number, ϑ^α is the azimuthual angle which leads to atom α, and:

$$\nu_n(r_n) = E_{AB}(r_n) - \frac{1}{2}\left[E_{AA}(r_n) + E_{BB}(r_n)\right], \tag{3.12}$$

where E_{AA}, E_{BB} and E_{AB} are the inter-atomic potentials for the n-th coordination shell which, for simplicity, are supposed to depend only of the radial distance, r_n. Second, again for simplicity, a two-dimensional arrangement of atoms is considered. This is shown in Figure 4 where a representative atom (shaded in gray color) is surrounded by first and second order neighbors (in black). Typical distances relevant

[6]For these they change slightly according to Vegard's law (see Predel, 1991-1997, pg. 185, or Lee and Raynor, 1955).

for lead and tin are also shown. The various sums of eqns (3.11) are approximately evaluated up to second neighbors to yield:

$$a^{\alpha} \approx \frac{4}{3}\left(r_1^{\mathrm{Sn}}\right)^2\left[\nu^{\mathrm{Pb}}\left(r_1^{\mathrm{Sn}}\right)+3\nu^{\mathrm{Pb}}\left(\sqrt{2}\,r_1^{\mathrm{Sn}}\right)\right],$$

$$a_1^{\beta} \approx 10\left(r_1^{\mathrm{Sn}}\right)^2\nu^{\mathrm{Sn}}\left(2r_1^{\mathrm{Sn}}\right), \qquad a_3^{\beta} = 2\left(r^{\mathrm{Pb}}\right)^2\left[\nu^{\mathrm{Sn}}\left(r_1^{\mathrm{Sn}}\right)+2\nu^{\mathrm{Sn}}\left(2r_1^{\mathrm{Sn}}\right)\right] \quad (3.13)$$

In here an average value of $2r_1^{\mathrm{Sn}}$ has been used to assess atoms number 3 to 10 which are shown in Figure 4. Following Cahn and Hilliard (1958), p. 263 it is now assumed for further evaluation that:

$$\nu^{\mathrm{Pb}}, \nu^{\mathrm{Sn}} \sim \frac{1}{r_n^6} \qquad (3.14)$$

which leads to roughly:

$$a^{\alpha} : a_1^{\beta} : a_3^{\beta} = 1.5 : 1 : 14. \qquad (3.15)$$

It should explicitly be pointed out that it is this difference in surface tension data which leads to the formation of eutectic lamellae.

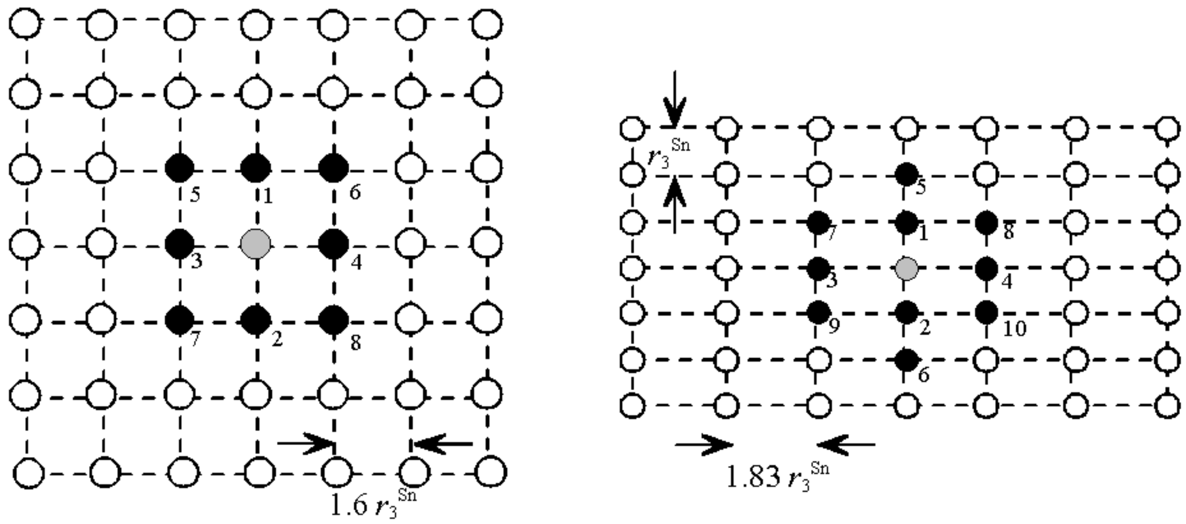

Fig. 4 2D-arrangements of a cubic lattice of Pb-atoms (left) and a tetragonal lattice of Sn-atoms (right), see text.

- In the very early stages of the phase separation the interfaces of the tin and lead rich regions will be coherent. However, when the equilibrium concentrations are approached the huge differences in the lattice constants between lead and tin (cf., eqn (3.10)) will only permit incoherent interfaces to exist. Raghavan and Cohen (1975), pp. 77, report that the specific surface energy, γ, of incoherent interfaces is in the range of:

$$\gamma \approx 0.5 - 1.5\frac{N}{m}, \qquad (3.16)$$

the maximum value of which was used for the simulations. In order to relate this information on specific surface energy, γ, to the coefficients $a^{\alpha}, a_1^{\beta}, a_3^{\beta}$, of eqn (3.15) the following definition is used (see also McFadden *et al.*, 1993, p. 2017, and the Appendix):

$$\begin{aligned} 2\gamma O &= \int_v \kappa^1_{ij} \frac{\partial^2 c}{\partial x_i \partial x_j} dV = \int_v \frac{\partial}{\partial x_i}\left(\kappa^1_{ij}\frac{\partial c}{\partial x_j}\right) dV - \int_v \frac{\partial \kappa^1_{ij}}{\partial x_i}\frac{\partial c}{\partial x_j} dV \\ &= \oint_O N_i \kappa^1_{ij} \frac{\partial c}{\partial x_j} dA - \int_v \frac{\partial \kappa^1_{ij}}{\partial x_i}\frac{\partial c}{\partial x_j} dV \end{aligned} \tag{3.17}$$

where r is the volume surrounded by the interface O, the normal unit vector of which is given by . As customary, the surface integral will be neglected in a large crystal. To evaluate the remaining part we put similarly to eqns (2.5), (2.7)-(2.9):

$$\kappa^1_{ij} = \kappa^\beta_{ij} - \frac{c^\beta - c}{c^\beta - c^\alpha}\left(\kappa^\beta_{ij} - \kappa^\alpha_{ij}\right) = -\left[\bar{\kappa}^\beta_{ij} - \frac{c^\beta - c}{c^\beta - c^\alpha}\left(\bar{\kappa}^\beta_{ij} - \bar{\kappa}^\alpha_{ij}\right)\right] c, \tag{3.18}$$

where it was defined (see eqns (A.35) and (A.36)):

$$\bar{\kappa}^\alpha_{ij} = \frac{1}{2}\omega\lambda^2\delta_{ij}, \quad \bar{\kappa}^\beta_{ij} = \frac{1}{2}\omega\begin{pmatrix} \lambda^2_a & 0 & 0 \\ 0 & \lambda^2_a & 0 \\ 0 & 0 & \lambda^2_b \end{pmatrix}. \tag{3.19}$$

Consequently:

$$\frac{\partial \kappa^1_{ij}}{\partial x_i} = -\frac{\partial c}{\partial x_i}\left[\bar{\kappa}^\beta_{ij} - \frac{c^\beta - 2c}{c^\beta - c^\alpha}\left(\bar{\kappa}^\beta_{ij} - \bar{\kappa}^\alpha_{ij}\right)\right]. \tag{3.20}$$

For further numerical evaluation it is now assumed that the second part in the bracket can be neglected, i.e., the properties of the α and of the β-phase are supposed to be similar, and, moreover, isotropy is assumed (see eqn (A.35)):

$$\frac{\partial \kappa^1_{ij}}{\partial x_i} = -a\frac{\partial c}{\partial x_i}\delta_{ij}. \tag{3.21}$$

Hence the following relation is obtained:

$$\gamma = \frac{a}{2O}\int_V \left(\frac{\partial c}{\partial x_i}\right)^2 dV, \tag{3.22}$$

Next it is assumed that the concentration gradient within the interface is linear and that equilibrium concentrations, c^α and c^β, have been reached within and outside of V. Then the following relation is easily derived:

$$a = 2\gamma\frac{\Delta x}{c^\beta - c^\alpha}. \tag{3.23}$$

For the numerical computations the width of the interface, Δx, was taken to be 50 atomic distances, i.e., in view of eqn (3.10) roughly 25nm. Note that because of the form of the phase diagram shown in Figure 2, the difference $c^\beta - c^\alpha$ and, consequently, the coefficient a depends on temperature. The value computed according to eqn (3.23) was chosen for the coefficient a^β_1 and the remaining two other coefficients were then related to it by means of eqn (3.15).

3.2 Low *vs.* high temperature aging without mechanical effects

In this subsection all mechanical effects of the development of the microstructural development are excluded. In other words, the two last terms in the equation for the diffusion flux (2.38) are switched off completely. Figures 6 and 7 show the temporal development of the microstructure of an originally homogeneous composition of Pb/Sn with six slight concentric disturbances/fluctuations of the eutectic concentration at 61.9%. The initial configuration is shown in Figure 5. All morphology sequences shown in this paper refer to 0.05, 0.1, 0.25, 0.5, 1.0, 2.5, 5.0 and 10.0 time units. The time step chosen was 10^{-4} and the dimensions of the RVE are roughly 1.5 microns. The initial composition is quenched from 183°C down to the high and low temperature levels of eqn (3.5) and (3.6), respectively. A thickening of the lamellae which is characteristic to the eutectic composition is clearly visible. It also appears that the lamellae are slightly thicker for the higher temperature.

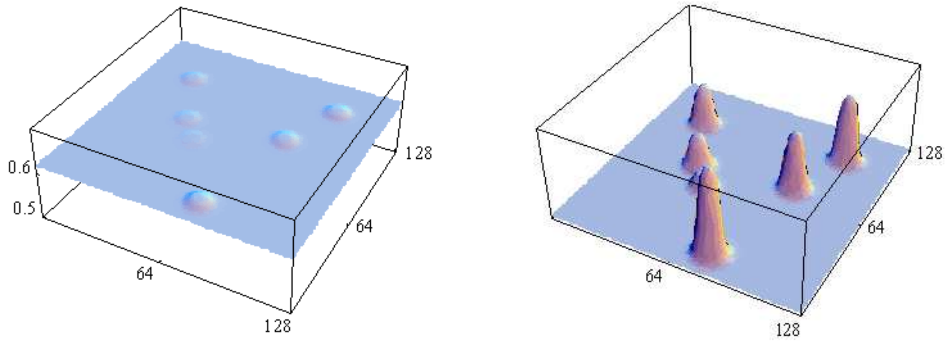

Fig. 5 Initial condition (the picture on the right is the magnified version of the picture on the left).

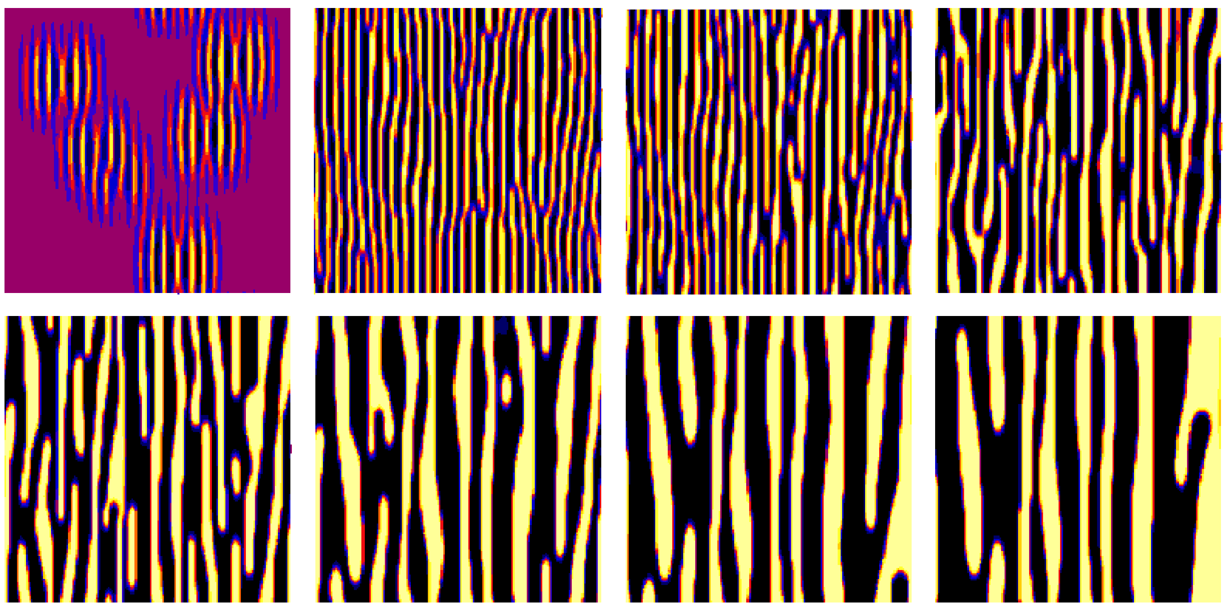

Fig. 6 Quenching from 183°C to 150°C, no mechanical contributions.

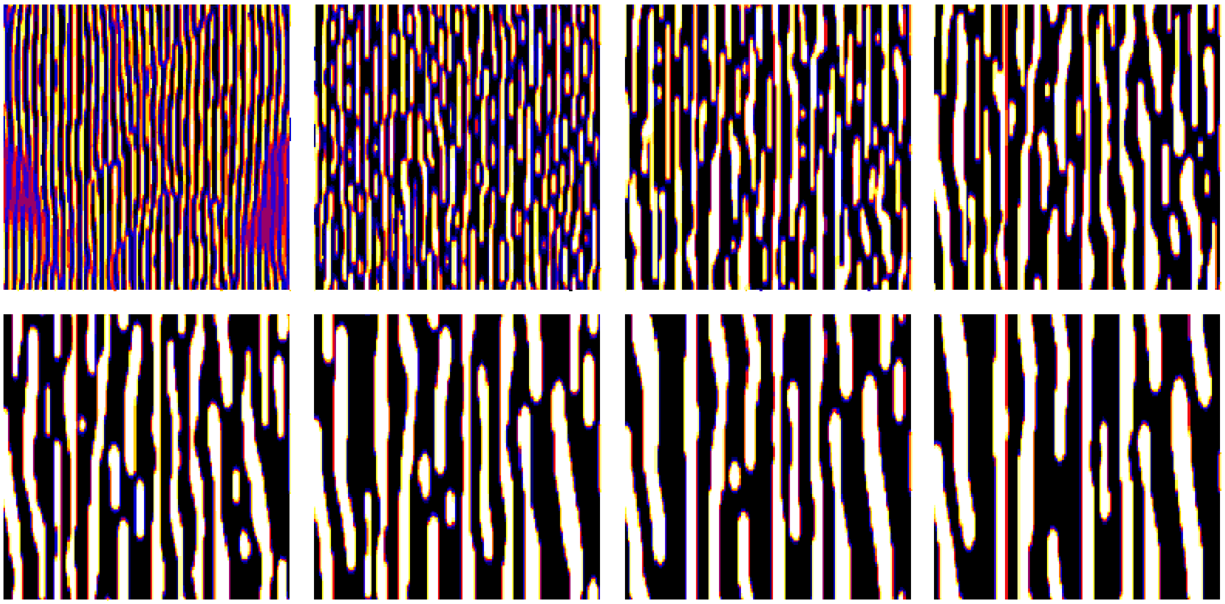

Fig. 7 Quenching from 183°C to 20°C, no mechanical contributions.

To a certain degree this behavior can be linked to experimental observations. Figure 8 shows micrographs from the work of Harris *et al.* (1991). According to these the lamellae thicken at room temperature as well as at elevated temperature levels. They are clearly thicker in the high temperature case. Also, when compared to the numerical simulation, the characteristic dimensions, such as spacing or thickness, differ by an order of magnitude. This is clearly due to the insufficient knowledge of the material parameters which were used during the simulation. It should also be noted that the experimental pictures exhibit all effects, in particular the influence of thermo-mechanical stresses. Moreover, an experiment is always three-dimensional which might also explain some of the discrepancies.

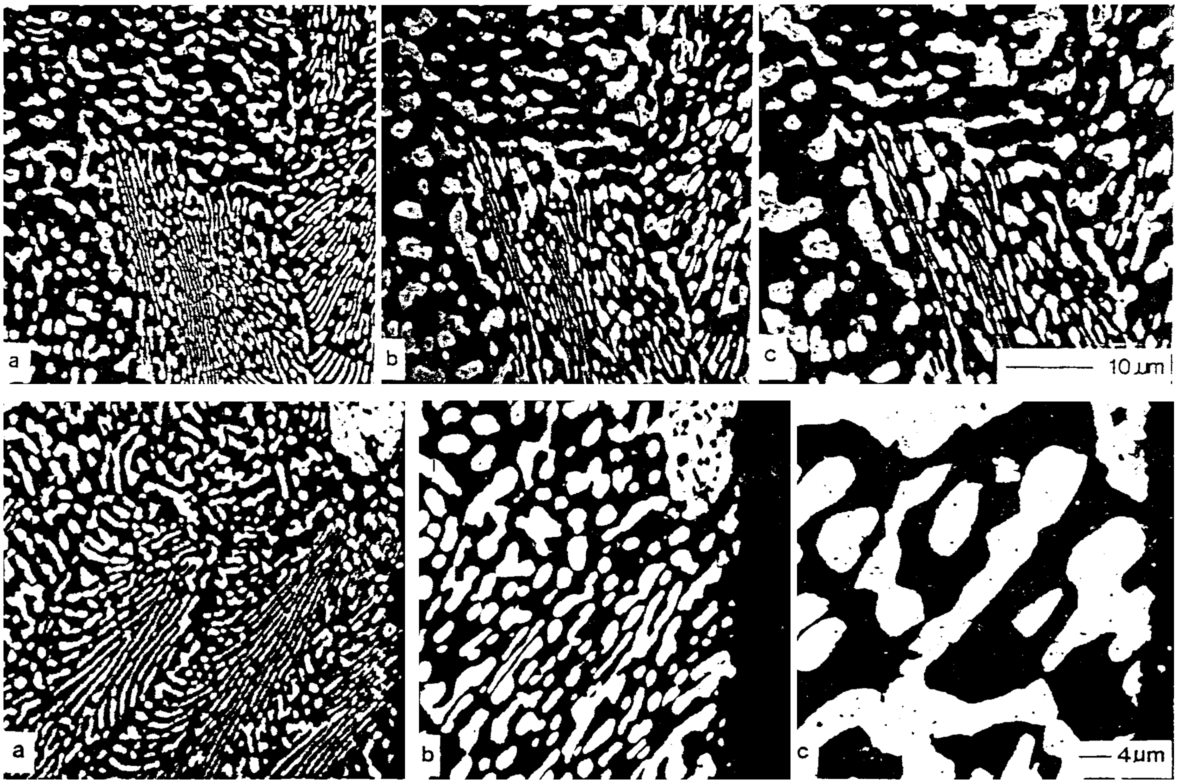

Fig. 8 Coarsening in a eutectic tin-lead solder, top row: effect of room temperature aging after (a) 2 hours, (b) 17 days, and (c) 63 days after solidification; bottom row: (a) immediately after solidification, (b) after 3 hours at and (c) 300 hours at 125°C.

However, it can clearly be stated that the development of lamellae in the numerical simulation is due to the use of an anisotropic surface tension according to eqn (3.15). If the same factor 1.5 is used for all directions and all phases the microstructural development is clearly more isotropic as shown in the sequence of Figure 9.

Fig. 9 Quenching from 183°C to 20°C, no mechanical contributions, isotropic surface tension.

The sequence in Figure 10 simulates the effect of thermal cycling on Pb/Sn solder. The first two rows show what happens if the temperature is changed from 20°C $\longrightarrow$ 150°C (where the microstructure of the last plot from Figure 7 has been used as the initial condition). Obviously an increase in temperature leads to a further coarsening of the lamellae which, as further simulations show, seems to irreversibly remain and even slightly increases after cooling to the original starting point. However, this might depend on the duration of the hold time, and it is certainly also affected by the presence of external loads, as will be shown in the next subsection.

Fig. 10 Quenching from 20°C $\longrightarrow$ 150°C $\longrightarrow$ 20°C, no mechanical contributions.

3.3 Low *vs.* high temperature aging with mechanical effects.

The sequence in Figure 11 is the same as in Figure 6 but with thermal stresses. No external loads were applied. The difference between them is not very large. The lamellae in Figure 11 appear slightly thicker. Whether this means that the chosen set of material parameters for the thermal stresses is incorrect and, if so, in which way it has to be corrected, or how the model must be modified is hard to decide since the thermal mismatch between the phases cannot be eleminated during an experiment. A possible way of how to get a better grip at this problem is to run aging experiments with other types of solders the phases of which should have different thermal expansion as well as stiffnesses. If the same type of thermal stress model would then be applied to describe their coarsening there is hope that by a relative comparison a decision could be made. It should also be mentioned that even though additional strain gradient terms are listed in the Appendix they were, up to now, not considered in the simulations. These will be closer examined in a forthcoming paper by the authors.

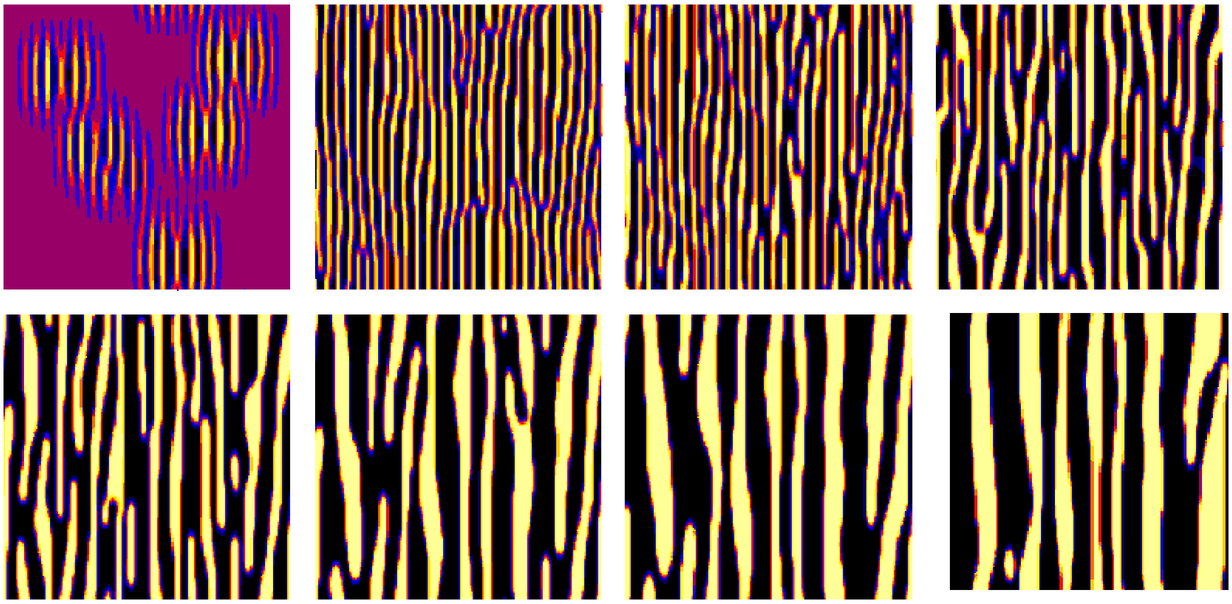

Fig. 11 Quenching from 183°C to 150°C, thermal stresses, no external loads.

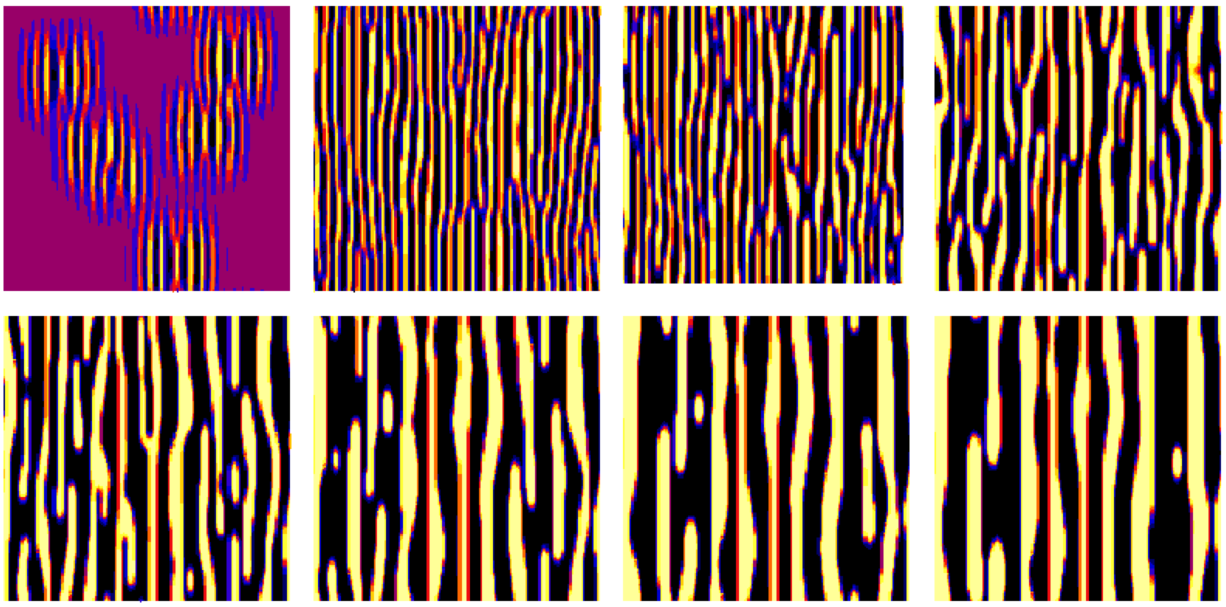

Fig. 12 Quenching from 183°C to 150°C, thermal stresses, external load $5 \cdot \Psi_0$ in horizontal direction.

Figure 12 presents a sequence of simulated micrographs where in addition to the thermal loads an additional external load of $5 \cdot \Psi_0$ has been applied in horizontal direction. For binary alloys Ψ_0 is typically in the order of 100 MPa. Hence, absolutely speaking, the load could be as high as 500 MPa which could not be supported by a SnPb solder. Indeed, further experimental research seems necessary to clarify this issue. However, for the time being the simulation shows that, provided they are sufficiently high, external stresses have an influence on the development of the microstructure of SnPb solder. In the present case they tend to thicken and misalign the lamellae at certain points. A certain delay in the evolution of a regular lamellae structure can also be observed.

3.4 Misalignment with respect to the main crystallographic axes

The sequence of Figure 13 is presented to show that the presented method is capable to simulate a eutectic SnPb lamella-structure which is not parallel to the main crystallographic axes. In fact it should be possible to model differently oriented grain regions. However, in view of the insufficient knowledge regarding many material parameters this should become a second step toward the perfection of the modeling of solders.

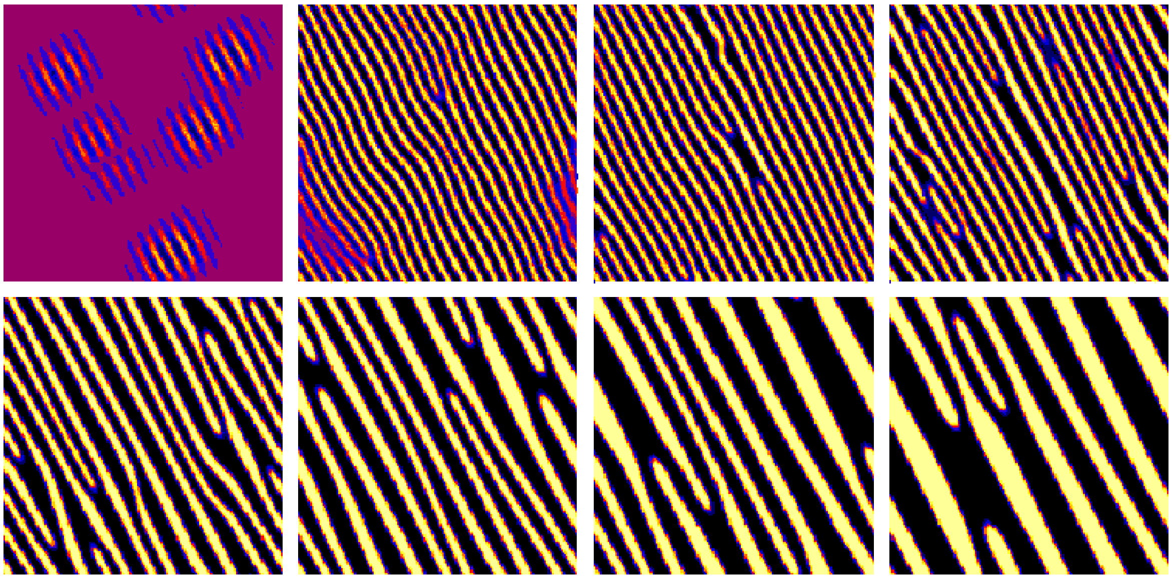

Fig. 13 Eutectic structure at an angle of 30° with respect to the main crystallographic axes.

4 Conclusions

The following issues were discussed in this paper:

- A purely continuum model can be devised and used to describe phase separation processes on a micro-morphological scale that are driven by diffusion through temperature, surface tensions, as well as local thermo-mechanical stresses and strains.
- This model has been successfully used for a qualitative modeling of the phase separation and coarsening process in binary eutectic tin-lead solders that are subjected to change in temperature and external as well as internal mechanical stresses.

- Arguments on the atomic scale can be used to gain additional information on material quantities such as the relative ranking of the components of the matrix of surface tension related quantities.

- The entropy principle can be used, together with atomistic arguments, to rationally derive the appropriate expressions for the stress-coupled diffusion flux.

- Discrete Fourier transforms can most effectively be used to solve mechanical as well the diffusion problems encountered during changes of micro-morphology. The corresponding theory was outlined and applied to the case of eutectic tin lead solders.

Acknowledgements. The foundations to this paper were laid during two visits of W.D. to the Department of Mechanical and Chemical Engineering at Heriot-Watt University and of W.H.M. to the Weierstraß Institute in June 1998. The stays was financially supported by Heriot-Watt University and by the British Council.

References

[1] Albrecht, H.-J., Gamalski, J. (1996). Fatigue properties of BGA solder joints: a comparison of thermal and power cycle Tests. Proc. SMI '96, San Jose, 61-80.

[2] Cahn, J.W., Hilliard, J.E. (1958). Free energy of a non-uniform system. I. Interfacial free energy. The Journal of Chemical Physics, 28 (1), pp. 258-267.

[3] Callister, W.D. Jr. (1997). Materials Science and Engineering - An Introduction. John Wiley Sons, Inc., New York.

[4] Canuto, C., Hussaini, M.Y., Quateroni, A., Zang, T.A. (1988). Spectral methods in fluid dynamics. Springer Series in Computational Physics. Springer Verlag, New York.

[5] Darveaux, R., Banerji, K., Mawer, A., and Dody, G. (1995). Reliability of plastic ball grid array assembly. In: Ball Grid Array Technology. (J. H. Lau). SMTnet, pp. 380-442.

[6] De Fontaine, D. (1975). Clustering effect in solid solutions. In: Treatise on Solid State Chemistry. (N.B. Hannah, editor). Plenum Press, New York, London, pp. 129-178.

[7] Dreyer, W. (1994). Development of microstructure based viscoplastic models for an advanced design of single crystal hot section components. In: Development of Microstructural Based Viscoplastic Models for an Advanced Design of Single Crystal Hot Section Components (J. Olschewski, ed.). Brite/Euram Per. Prog. Rpt., pp. A.1-17-A.1-29.

[8] Dreyer, W., Müller, W.H., Olschewski, J. (1998). An Approximate Analytical 2D-Solution for the Stresses and Strains in Eigenstrained Cubic Materials, Acta Mechanica, in print.

[9] Falk, G. (1966). Theoretische Physik auf der Grundlage einer allgemeinen Dynamik, Band I a Aufgaben und Ergänzungen zur Punktmechanik, Springer, Berlin Heidelberg New York.

[10] Hacke, P.L., Sprecher, A.F., Conrad, H. (1997). Microstructure coarsening during thermo-mechanical fatigue of PbSn solder joints. Journal of Electronic Materials, 28 (7), pp. 774-782.

[11] Handbook of Chemistry and Physics. (1995). 76th Edition, CRC, The Chemical Rubber Co., Cleve-land, Ohio.

[12] Harris, P.G., Chaggar, K.S., Whitmore, M.A. (1991). The effect of ageing on the microstructure of 60:40 tin-lead solders. Soldering and Surface Mount Technology, 7, pp. 20-23.

[13] Hauck, T., Müller, W.H., Albrecht, H.J., Gamalski J. (1996). Concepts Toward Lifetime Analysis of BGA Structures, '96 Proc. Surface Mount International, San Jose, September 10-12, 1996, Volume I, pp. 109-120.

[14] Hawick, K.A. (1991). Domain growth in alloys. PhD-thesis, Edinburgh University.

[15] Hwang, J.S., Lucey, G. (1993) Strengthened solder materials for electronic packages. In: Proceedings of the Surface Mount International, pp. 662-676.

[16] Flanders, D.R., Jacobs, E.G., Pinizotto, R.F. (1997). Activation energies of intermetallic growth of Sn-Ag eutectic solder on copper substrates. Journal of Electronic Materials, 26 (7), pp. 883-887.

[17] Jendrny, J., Müller, W.H., Albrecht, H.-J. (1997). Strength and lifetime analysis of SMT solder joints: An exemplary study of the MiniMelf component. Proc. Surface Mount International Conference, San Jose, pp. 626-636.

[18] Khachaturyan, A.G., Semenovskaya, S., Tsakalakos, T. (1995). Elastic strain energy of inhomogene-ous solids. Physical Review B. 52(22), pp. 15909-15919.

[19] Koyama, T., Miyazaki, T. (1994). Computer simulation of phase decomposition in real alloy systems. In: Solid $\rightarrow$ Solid Phase Transformations, Editors: W.C. Johnson, J.M. Howe, D.E. Laughlin and W.A. Soffa, The Minerals, Metals & Materials Society, pp. 365-370.

[20] Koyama, T., Miyazaki, T. (1998). Computer simulation of phase decomposition in two dimensions based on a discrte type non-linear diffusion equation. Materials Transactions, JIM. 39(1), pp. 169-178.

[21] Koyama, T., Miyazaki, T., Mebed, A.E.-A. M. (1994). Computer Simulations of phase decomposition in real alloy systems based on the modified Khachaturyan diffusion equation. Metallurgical and Materials Transactions A. 26A, pp. 1995-2617.

[22] Koyama, T., Miyazaki, T., Doi, M., Mebed, A. E.-A. M., Moriya, T. (1996). Computer simulation of phase decomposition in Fe-Mo alloy based on discrete type diffusion equation. J. Japan. Inst. Met-als. 60(6), pp. 560-568.

[23] Küpper, T., Masbaum, N. (1994). Simulation of particle growth and Ostwald ripening via the Cahn-Hilliard equation. Acta metall. Mater. 42(6), pp. 1847-1858.

[24] Laberge, C.A., Fratzl, P., Lebowitz, J.L. (1997). Microscopic model for directional coarsening of precipitates in alloys under external load. Acta. Mater. 45(10), pp. 3949-3961.

[25] Lau, J.H., Rice, D.W. (1985). Solder Joint Fatigue in Surface Mount Technology: State of the Art. Solid State Technology, pp. 91-104.

[26] Lee, J.A., Raynor, G.V. (1955). The lattice spacings of binary tin-rich alloys. Proc. Phys. Soc. LXVII, 10-B, 737-747.

[27] Li, D.Y., Chen, L.Q. (1997). Computer simulation of morphological evolution and rafting of particles in Ni-based superalloys under applied stress, Scripta Materialia, 37(9), pp. 1271-1277.

[28] Logsdon, W.A., Liaw, P.K., Burke, M.A. (1990). Fracture behavior of 63Sn-37Pb solder. Engineering Fracture Mechanics, 36 (2), pp. 183-218.

[29] Massalski, T.B. (1965). Structure of solid solutions. In: Physical Metallurgy (Edited by R.W. Cahn). North-Holland Publishing Company, Amsterdam.

[30] McCormack, M., Khachaturyan A.G. and Morris Jr, J.W. (1992). A two-dimensional analysis of the evolution of coherent precipitates in elastic media. Acta metall. mater. 40 (2), pp. 325-336.

[31] McFadden, G.B., Wheeler, A.A., Braun, R.J., Coriel, S.R. (1993). Phase-field models for anisotropic interfaces. Physical Review E, 48 (3), pp. 2016-2024.

[32] Mebed, A.M., Koyama, T., Miyazaki, T. (1997). Computer simulation of A2/B2 second-order phase transition based upon the Khachaturyan diffusion equation. Journal of Materials Science 32, pp. 5797-5804.

[33] Miyazaki, T., Koyama, T. (1996). Theoretical analysis of phase decomposition in real alloy systems based on the non-linear diffusion equation. Materials Transactions, JIM. 37(4), pp. 684-690.

[34] Miyazaki, T., Koyama, T. (1997). Computer simulation of microstructure formation of the real alloy systems based on the discrte type non-linear diffusion equation. In: Proceedings of the Workshop "Recent Developments in the Study of Irreversible Processes," 18-19 September 1997, Nagoya In-stitute of Technology, editor M. Sugiyama. pp. 79-85.

[35] Miyazaki, T., Takeuchi, A., Koyama, T., Kozakai, T. (1991). Computer simulation of phase decom-position in the regular solid solution based upon the Chan-Hilliard's non-linear diffusion equation. Materials Transactions, JIM. 32(10), pp. 915-920.

[36] Moulinec, H. and Suquet, P. (1994). A fast numerical method for computing the linear and nonlinear mechanical properties of composites, C. R. Acad. Sci. Paris, 318 (II), 1417-1423.

[37] Moulinec, H. and Suquet, P. (1998). A numerical method for computing the overall response of nonlinear composites with complex microstructure, Comp. Meth. Appl. Mech. Engng., in print.

[38] Müller, I. (1985). Thermodynamics. Pitman, Boston, London, Melbourne.

[39] Müller, W.H. (1996). Mathematical vs. experimental stress analysis of inhomogeneities in solids. Journal de Physique IV. Colloque C1, supplément au Journal de Physique III, 6, C1-139-C1-148.

[40] Müller, W.H. (1998a). Fourier transforms and their application to the formation of textures and changes of morphology in solids, Proc. IUTAM Symp. on Transformation Problems in Composite and Active Materials, Cairo, in press.

[41] Müller, W.H. (1998b): The possibilities of Fourier transforms for the calculation of damage evolution in metals, ZAMM, in print.

[42] Müller, W.H., Neumann, S. (1998). An approximate analytical 3D-solution for the stresses and strains in eigenstrained cubic materials. Int. J. Sol. Struct., 35 (22), pp. 2931-2958.

[43] Mura, T. (1987) Micromechanics of Defects in Solids, second revised edition, Martinus Nijhoff Publishers, Dordrecht, The Netherlands.

[44] Nishimori, H., Onuki, A. (1990). Pattern formation in phase-separating alloys with cubic symmetry. Physical Review B, 42(1), pp. 980-983.

[45] Nylén, M., Hutchinson, B., and Gustavsson, U. (1997). Microstructural degradation of solder. In: Proc. Micro Materials, Micro Mat Š97, Berlin, pp. 890-895.

[46] Ozmat, B. (1990). A nonlinear thermal stress analysis of surface mount solder joints. Proc. 40th IEEE ECTC, Vol. II, pp. 959-972.

[47] Pao, Y.-H. (1992). A fracture mechanics approach to thermal fatigue life prediction of solder joints. IEEE Transactions on Components, Hybrids, and Manufacturing Technology, 15(4), pp. 559-570.

[48] Predel, B. (1991-1997). Phase Equilibria, Crystallographic and Thermodynamic Data of Binary Al-loys, volume 5, subvolume I Ni-Np...Pt-Zr. Springer , Berlin, Germany.

[49] Raghavan, V., Cohen, M., (1975). Solid-State Phase Transformations, in: Treatise on Solid State Cheistr, Volume 5, Changes of State, (N.B. Hannay, editor), Plenum Press, New York-London, pp. 67-127.

[50] Raynor, G.V. (1965). Phase diagrams and their determination. In: Physical Metallurgy (Edited by R.W. Cahn). North-Holland Publishing Company, Amsterdam, pp. 291-363.

[51] Rothman, S.J. (1984). The measurement of tracer diffusion coefficients in solids. In: Diffusion in Crystalline Solids (J.E. Murch, A.S. Nowick, eds.). Academic Press, Inc. Orlando, pp. 1-61.

[52] Seyyedi, J., Arsenault, B., and Keller, J.P. (1991). Stress-rupture and creep behaviour of 63Sn-37Pb production soldered connections. Soldering & Surface Mount Technology, 7, pp.49-55.

[53] Sundquist, B.E. (1964). A direct determination of the anisotropy of the surface free energy of solid gold, silver, copper, nickel, and alpha and gamma iron. Acta Metallurgica. 12, pp. 67-86.

[54] Suquet, P. (1990). Une méthode simplifiée pour le calcul de propriétés élastiques de matériaux hétérogènes à structure périodique, C. R. Acad. Sci. Paris. 311 (II), 769-774.

[55] Tsakalakos, T. (19). On certain phase transition related problems in metallurgy. In: . pp. 149-184.

[56] Wang, Y. and Khachaturyan, A.G. (1995). Shape instability during precipitate growth in coherent solids, Acta metall. Mater., 43 (5), pp. 1837-1857.

[57] Wang, Y., Khachaturyan, A.G. (1997). Three-dimensional Field Model and computer modeling of martensitic transformations. Acta metall. Mater. 45 (2), pp. 759-773.

[58] Wang, Y., Chen, L.-Q., Khachaturyan, A.G. (1991). Strain-induced modulated structures in two-phase cubic alloys. Scripta Metallurgica et Materialia. 25, pp. 1969-1974.

[59] Wang, Y., Chen, L.-Q., Khachaturyan, A.G. (1993a). Kinetics of strain-induced morphological trans-formation in cubic alloys with a miscibility gap. Acta metall. mater. 41(1), pp. 279-296.

[60] Wang, Y., Wang, H., Chen, L.-Q., Khachaturyan, A.G. (1993b). Shape evolution of a coherent tetragonal precipitate in partially stabilized cubic ZrO2: A computer simulation. The journal of the American Ceramic Society. 76(12), pp. 3029-3033.

[61] Wang, Y., Wang, H., Chen, L.-Q., Khachaturyan, A.G. (1994). Computer simulation of microstruc-ture evolution in coherent solids. In: Solid $\rightarrow$ Solid Phase Transformations, Editors: W.C. Johnson, J.M. Howe, D.E. Laughlin and W.A. Soffa, The Minerals, Metals & Materials Society, pp. 245-265.

[62] Winter, M. (1998). WebElements & trade;. University of Sheffield, http://www.shef.ac.uk/chemistry/web-elements/.

A A modicum of thermodynamics

In this paper the following field variables are of primary interest:

motion:

$$x_i = \tilde{x}_i(X_k, t), \qquad i, j \in \{1, 2, 3\}, \tag{A.1}$$

the concentrations of all constituents of the mixture:

$$c^A = \frac{\tilde{\rho}_0^A(X_k, t)}{\tilde{\rho}_0(X_k, t)}, \tag{A.2}$$

and the temperature:

$$T = \tilde{T}(X_k, t). \tag{A.3}$$

The symbols X_k indicate the material coordinates of a continuum particle, t denotes the time, the subscript A identifies the constituent, and ρ_0^A and ρ_0 are the mass densities with respect to the reference configuration of constituent A and of the total mass, respectively. The following relations hold for the current total mass density, ρ, and for the current partial mass densities, ρ^A, (Müller, 1985, p. 61, p. 71):

$$\rho = \frac{\rho_0}{\det \underline{F}}, \qquad \rho = \sum_A \rho^A, \tag{A.4}$$

where $\underline{F}$ denotes the deformation gradient:

$$F_{ij} = \frac{\partial \tilde{x}_i}{\partial X_j}. \tag{A.5}$$

Sometimes it happens that the solid in the reference configuration consists already of two phases, α and β. In this case we write:

$$\rho_0 = \rho_0^\beta - (\rho_0^\beta - \rho_0^\alpha)\tilde{\theta}(X_k, t), \tag{A.6}$$

with

$$\tilde{\theta}(X_k, t) = \frac{c^\beta - \tilde{c}(X_k, t)}{c^\beta - c^\alpha}. \tag{A.7}$$

Within this section on thermodynamics the right Cauchy-Green tensor, C_{ij}, is used as a general strain measure instead of the infinitesimal strain, ε_{ij}:

$$C_{ij} = F_{ki}F_{kj} \approx 1 + 2\varepsilon_{ij} \quad \text{for} \quad |\varepsilon_{ij}| \ll 1. \tag{A.8}$$

The solution for the field variables is based on the balance equations for the concentration, c:[7]

$$\rho_0 \dot{c} + \frac{\partial J_k}{\partial X_k} = 0, \tag{A.9}$$

momentum:

$$\rho_0 \dot{v}_i - \frac{\partial t_{ik}}{\partial X_k} = 0, \tag{A.10}$$

[7]For simplicity a binary mixture with no chemical reactions was assumed and the index A is omitted from now on.

and for internal energy, u:

$$\rho_0 \dot{u} + \frac{\partial Q_k}{\partial X_k} = t_{ik} \frac{\partial v_i}{\partial X_k} \equiv \frac{1}{2} T_{ij} \dot{C}_{ij}. \tag{A.11}$$

In these equations dots refer to material time derivatives, J_k denotes the diffusion flux, t_{ik} and T_{ij} are the first and second Piola-Kirchhoff stress tensors, respectively, and Q_k is the material heat flux (Müller, 1985, p. 77). If the differences between the current and the reference configuration are ignored, as it is customary for small deformations and as it was done during the simulations presented in this paper, there is no difference between t_{ik} and T_{ij}, and both tensors can be approximated by the Cauchy stress tensor, σ_{ij}.

Note that in the simulations presented in this paper the acceleration terms, $\rho_0 \dot{v}_i$, in the balance of momentum were neglected and the balance of internal energy was completely ignored since the temperature field was prescribed as constant and homogeneous throughout the solder.

The balance equations become field equations if the quantities J_i, T_{ij} (or t_{ij}), u, and Q_i are related to the variables in a material-dependent manner by constitutive equations. Restrictions for such equations are imposed by the local inequality for the specific entropy, s, which reads (Müller, 1985, p. 168):

$$\rho_0 \dot{s} + \frac{\partial \phi_k}{\partial X_k} = \Sigma \geq 0, \tag{A.12}$$

where ϕ_k is the entropy flux and Σ denotes the (positive) entropy production density which are also constitutive quantities, in the same manner as J_i, etc.

Note that this inequality holds exclusively for solutions of the field equations. These constraints are taken into account in the famous lemma by I-Shih Liu and Müller (see Müller, 1985, pp. 167) which allows for a straightforward derivation of all the restrictions imposed by the entropy principle on the constitutive relations. It states: If the entropy inequality (A.12) holds only for solutions of the field equations then:

$$\rho_0 \dot{s} + \frac{\partial \phi_k}{\partial X_k} - \Lambda^c \left(\rho_0 \dot{c} + \frac{\partial J_k}{\partial X_k} \right) - \Lambda_i^v \left(\rho_0 \dot{v}_i - \frac{\partial t_{ik}}{\partial X_k} \right) - \Lambda^u \left(\rho_0 \dot{u} + \frac{\partial Q_k}{\partial X_k} - \frac{1}{2} T_{ij} \dot{C}_{ij} \right) \geq 0 \tag{A.13}$$

must hold for arbitrary fields of concentration, motion, and temperature. The symbols Λ^c, Λ_i^v, Λ^u are Lagrange multipliers which may depend on all independent variables including their derivatives. The inequality must now be exploited in order to arrive at reduced, preferably explicit, forms for u, J_k, T_{ij}, Q_k in terms of the fields c, $\underline{C}$, T and their derivatives.

The general exploitation of eqn (A.13) will be presented in another paper by the authors. It turns out that the effort during this exploitation can be reduced considerably if it is assumed, motivated by experience, that:

$$\Lambda^u = \frac{1}{T}. \tag{A.14}$$

Motivated by arguments from statistical mechanics (Cahn and Hilliard, 1958, pp. 262) the specific free energy, $\psi = u - Ts$, of the binary alloy is a *known* function of the following variables:

$$\psi = \tilde{\psi} \left(c, \frac{\partial c}{\partial X_k}, \frac{\partial^2 c}{\partial X_k, \partial X_s}, C_{ij}, \frac{\partial C_{ij}}{\partial X_k}, \frac{\partial^2 C_{ij}}{\partial X_k \partial X_s}, T \right), \tag{A.15}$$

Consequently, the inequality is linear with respect to $\dot{v}_i$ and, therefore:

$$\Lambda_i^v = 0, \tag{A.16}$$

must hold since otherwise the inequality could easily be violated. Insertion of these eqns into eqn (A.14)-(A.16) and performing the differentiations yields:

$$\frac{\rho_0}{\Lambda^u}\left(s+\frac{\partial\psi}{\partial T}\right)\dot{\Lambda}^u - \rho_0\Lambda^u\left(\frac{\partial\psi}{\partial c}+\frac{\Lambda^c}{\Lambda^u}\right)\dot{c} - \rho_0\Lambda^u\left(\frac{\partial\psi}{\partial C_{ij}}-\frac{1}{2\rho_0}T_{ij}\right)\dot{C}_{ij} -$$
$$\rho_0\Lambda^u\frac{\partial\psi}{\partial(\partial c/\partial X_k)}\left(\frac{\partial c}{\partial X_k}\right)^{\bullet} - \rho_0\Lambda^u\frac{\partial\psi}{\partial(\partial C_{ij}/\partial X_k)}\left(\frac{\partial C_{ij}}{\partial X_k}\right)^{\bullet} - \tag{A.17}$$
$$\rho_0\Lambda^u\frac{\partial\psi}{\partial(\partial^2 c/\partial X_k\partial X_s)}\left(\frac{\partial^2 c}{\partial X_k\partial X_s}\right)^{\bullet} - \rho_0\Lambda^u\frac{\partial\psi}{\partial(\partial^2 C_{ij}/\partial X_k\partial X_s)}\left(\frac{\partial^2 C_{ij}}{\partial X_k\partial X_s}\right)^{\bullet} + \frac{\partial\phi_k'}{\partial X_k} \geq 0,$$

whith the definition:

$$\phi_k' = \phi_k - \Lambda^u Q_k - \Lambda^c J_k. \tag{A.18}$$

With the same kind of argument as above the linearity in $\dot{\Lambda}^u$ implies:

$$s = -\frac{\partial\psi}{\partial T}. \tag{A.19}$$

If the flux ϕ_k' is supposed to depend on the same variables as the free energy and all the other constitutive quantities then it can easily be shown that the free energy could only depend on c, C_{ij}, and T and *not* on their derivatives. On the other hand it is known from statistical mechanics that such a dependence exists. The simplest way to achieve consistency with the second law is to assume that:

$$\phi_k' = \varphi_k\dot{c} + \varphi_{kij}\dot{C}_{ij} + \varphi_{ks}\left(\frac{\partial c}{\partial X_s}\right)^{\bullet} + \varphi_{kijs}\left(\frac{\partial C_{ij}}{\partial X_s}\right)^{\bullet}, \tag{A.20}$$

where, in consistency with eqn (A.15), all coefficients φ may show a functional dependence as follows:

$$\varphi = \tilde{\varphi}\left(c, \frac{\partial c}{\partial X_k}, \frac{\partial^2 c}{\partial X_k, \partial X_s}, C_{ij}, \frac{\partial C_{ij}}{\partial X_k}, \frac{\partial^2 C_{ij}}{\partial X_k, \partial X_s}, T\right). \tag{A.21}$$

If eqn (A.20) is now inserted into (A.17) the following result is obtained:[8]

$$-\rho_0\Lambda^u\left(\frac{\partial\psi}{\partial c}+\frac{\Lambda^c}{\Lambda^u}-\frac{1}{\rho_0\Lambda^u}\frac{\partial\varphi_k}{\partial X_k}\right)\dot{c} - \rho_0\Lambda^u\left(\frac{\partial\psi}{\partial C_{ij}}-\frac{1}{2\rho_0}T_{ij}-\frac{1}{\rho_0\Lambda^u}\frac{\partial\varphi_{kij}}{\partial X_k}\right)\dot{C}_{ij} - \tag{A.22}$$
$$\left(\varphi_k+\frac{\partial\varphi_{ks}}{\partial X_k}-\rho_0\Lambda^u\frac{\partial\psi}{\partial(\partial c/\partial X_s)}\right)\left(\frac{\partial C}{\partial X_s}\right)^{\bullet} + \left(\varphi_{sij}+\frac{\partial\varphi_{kijs}}{\partial X_k}-\rho_0\Lambda^u\frac{\partial\psi}{\partial(\partial C_{ij}/\partial X_s)}\right)\left(\frac{\partial C_{ij}}{\partial X_s}\right)^{\bullet} +$$
$$\left(\varphi_{ks}-\rho_0\Lambda^u\frac{\partial\psi}{\partial(\partial^2 c/\partial X_k\partial X_s)}\right)\left(\frac{\partial^2 c}{\partial X_k\partial X_s}\right)^{\bullet} + \left(\varphi_{kijs}-\rho_0\Lambda^u\frac{\partial\psi}{\partial(\partial^2 C_{ij}/\partial X_k\partial X_s)}\right)\left(\frac{\partial^2 C_{ij}}{\partial X_k\partial X_s}\right)^{\bullet} +$$
$$+Q_k\frac{\partial\Lambda^u}{\partial X_k} + J_k\frac{\partial\Lambda^c}{\partial X_k} \geq 0,$$

[8]Because of their independence material time derivatives and spatial derivatives can simply be interchanged. This explains why a Lagrangian formulation was used.

The inequality (A.22) is linear in $\dot{c}$, $\dot{C}_{ij}$, $\left(\frac{\partial c}{\partial X_s}\right)^\bullet$, $\left(\frac{\partial C_{ij}}{\partial X_s}\right)^\bullet$ and, following the same line of arguments as above, it follows that:

$$\Lambda^c = -\frac{1}{T}\frac{\partial \psi}{\partial c} + \frac{1}{\rho_0}\frac{\partial \varphi_s}{\partial X_s}, \tag{A.23}$$

$$T_{ij} = 2\rho_0 \frac{\partial \psi}{\partial C_{ij}} - 2T\frac{\partial \varphi_{sij}}{\partial X_s}, \tag{A.24}$$

$$\varphi_s = -\frac{\partial \varphi_{ks}}{\partial X_k} + \frac{\rho_0}{T}\frac{\partial \psi}{\partial(\partial c/\partial X_s)}, \tag{A.25}$$

$$\varphi_{ks} = \frac{\rho_0}{T}\frac{\partial \psi}{\partial(\partial^2 c/\partial X_k \partial X_s)}, \tag{A.26}$$

$$\varphi_{kij} = -\frac{\partial \varphi_{kijs}}{\partial X_k} + \frac{\rho_0}{T}\frac{\partial \psi}{\partial(\partial C_{ij}/\partial X_s)}, \tag{A.27}$$

$$\varphi_{kijs} = \frac{\rho_0}{T}\frac{\partial \psi}{\partial(\partial^2 C_{ij}/\partial X_k \partial X_s)}. \tag{A.28}$$

There remains the residual inequality:

$$Q_k \frac{\partial \Lambda^u}{\partial X_k} + J_k \frac{\partial \Lambda^c}{\partial X_k} \geq 0. \tag{A.29}$$

If coupling between heat and diffusion is ignored the simplest way to satisfy eqn (A.29) is given by the choice:

$$Q_i = -\kappa_{ik}\frac{\partial T}{\partial X_k}, \qquad J_i = M_{ik} T \frac{\partial \Lambda^c}{\partial X_k}, \tag{A.30}$$

with two positive definite matrices, one for the thermal conduction coefficients, κ_{ik}, and one for the mobility coefficients, M_{ik}. After elimination of φ_k, φ_{ks}, φ_{kij}, and φ_{kijs} it follows that:

$$\begin{aligned} \Lambda^c = & -\frac{1}{T}\frac{\partial \psi}{\partial c} + \frac{1}{T}\frac{\partial}{\partial X_k}\left(\frac{\partial \psi}{\partial(\partial c/\partial X_k)}\right) + \frac{1}{\rho_0}\frac{\partial \psi}{\partial(\partial c/\partial X_k)}\frac{\partial}{\partial X_k}\left(\frac{\rho_0}{T}\right) - \\ & \frac{1}{T}\frac{\partial^2}{\partial X_k \partial X_s}\left(\frac{\partial \psi}{\partial(\partial^2 c/\partial X_k \partial X_s)}\right) - \frac{1}{\rho_0}\frac{\partial \psi}{\partial(\partial^2 c/\partial X_k \partial X_s)}\frac{\partial^2}{\partial X_k \partial X_s}\left(\frac{\rho_0}{T}\right), \end{aligned} \tag{A.31}$$

$$\begin{aligned} T_{ij} = & \, 2\rho_0 \frac{\partial \psi}{\partial C_{ij}} - 2\rho_0 \frac{\partial}{\partial X_k}\left(\frac{\partial \psi}{\partial(\partial C_{ij}/\partial X_k)}\right) - T\frac{\partial \psi}{\partial(\partial C_{ij}/\partial X_k)}\frac{\partial}{\partial X_k}\left(\frac{\rho_0}{T}\right) + \\ & 2\rho_0 \frac{\partial^2}{\partial X_k \partial X_s}\left(\frac{\partial \psi}{\partial(\partial^2 C_{ij}/\partial X_k \partial X_s)}\right) + 2T\frac{\partial \psi}{\partial(\partial^2 C_{ij}/\partial X_k \partial X_s)}\frac{\partial^2}{\partial X_k \partial X_s}\left(\frac{\rho_0}{T}\right). \end{aligned} \tag{A.32}$$

Thus the diffusion flux as well as the stress, which are the quantities of primary interest in this paper, are reduced to derivatives of the free energy alone. For the simulations discussed in this paper eqns $(A.30)_2$, (A.31), and (A.32) are the most important results of this section on thermodynamics. The reference configuration is often identified with the melt. For that choice the various ρ_0-terms in (A.31) and (A.32) drop out if, in addition, a homogeneous temperature distribution is assumed.

Following the statistical arguments present on pp. 263 of the paper by Cahn and Hilliard (1958) the following form of the specific free energy can be established if coupling between strain and concentrations on the micro-scale is ignored:

$$\psi = \psi' + \kappa^1_{ij} \frac{\partial^2 c}{\partial X_i \partial X_j} + \frac{1}{2} \kappa^2_{ij} \frac{\partial c}{\partial X_i} \frac{\partial c}{\partial X_j}. \tag{A.33}$$

In here ψ' is the configurational part of the free energy, which still includes strain ("elastic") energy, and the coefficients κ^1_{ij} and κ^2_{ij} are given by:

$$\kappa^2_{ij} = 0, \tag{A.34}$$

$$\kappa^1_{ij} = a\delta_{ij}, \qquad a = -\frac{1}{2}\omega\lambda^2 c \qquad \text{(for cubic crystals)}, \tag{A.35}$$

and:

$$\kappa^1_{ij} = \begin{pmatrix} a & 0 & 0 \\ 0 & a & 0 \\ 0 & 0 & b \end{pmatrix}, \quad a = -\frac{1}{2}\omega\lambda^2_a c, \quad b = -\frac{1}{2}\omega\lambda^2_b c \qquad \text{(for tetragonal crystals)}, \tag{A.36}$$

where:

$$\omega = \sum_n Z_n \nu_n, \; \nu_n = E_{AB}(r_n) - \frac{1}{2}(E_{AA}(r_n) + E_{BB}(r_n)), \; \lambda^2 = \frac{1}{3\omega} \sum_n Z_n r^2_n \nu_n, \tag{A.37}$$

$$\lambda^2_a = \frac{1}{2\omega} \sum_n \left(Z_n - \sum_{\alpha=1}^{Z_n} \cos^2(\vartheta^\alpha) \right) r^2_n \nu_n, \quad \lambda^2_b = \frac{1}{\omega} \sum_n \left(\sum_{\alpha=1}^{Z_n} \cos^2(\vartheta^\alpha) \right) r^2_n \nu_n. \tag{A.38}$$

Moreover, Z_n is the coordination number of the n-th coordination shell at a radius r_n from a refer-ence atom, E_{AA},E_{BB}, and E_{AB} denote the pairwise interaction potentials of a binary alloy, and ϑ^α is the azimuthal angle which starts from the tetragonal axis. If the temperature within the alloy is homogeneous and if the reference configuration is chosen to be the one of the melt, insertion of eqn (A.33) into eqn (A.34) leads to the following result for the diffusion flux of eqn $(A.30)_2$:

$$J_i = -M_{ij} \frac{\partial}{\partial X_j} \left(\frac{\partial \psi'}{\partial c} + \frac{\partial \kappa^1_{rs}}{\partial c} \frac{\partial^2 c}{\partial X_r \partial X_s} \frac{\partial^2 \kappa^1_{rs}}{\partial X_r \partial X_s} \right) = -M_{ij} \frac{\partial}{\partial X_j} \left(\frac{\partial \psi'}{\partial c} - a_{rs} \frac{\partial^2 c}{\partial X_r \partial X_s} \right), \tag{A.39}$$

where:

$$a_{ij} = \omega\lambda^2 \delta_{ij} \qquad \text{(for cubic crystals)}, \tag{A.40}$$

and:

$$a_{ij} = \omega \begin{pmatrix} \lambda^2_a & 0 & 0 \\ 0 & \lambda^2_a & 0 \\ 0 & 0 & \lambda^2_b \end{pmatrix} \qquad \text{(for tetragonal crystals)}. \tag{A.41}$$

In the simulations presented in this paper the contribution of strain gradients were neglected. Thus, the configurational part of the free energy, ψ', is additively split into a strain free configurational part, ψ_0, and another part, ψ_{def}, which contains the free energy stored due to the deformation, C_{ij}:

$$\psi' = \tilde{\psi}_0(c) + \tilde{\psi}_{\text{def}}(c, C_{ij}). \tag{A.42}$$

For a linear elastic body which is subjected to small deformations we write:

$$\psi_{\mathrm{def}} = \frac{1}{2}\left(\varepsilon_{ij} - \varepsilon^{*}_{ij}(c)\right) C_{ijkl}(c) \left(\varepsilon_{kl} - \varepsilon^{*}_{kl}(c)\right), \quad \text{where} \;\; \varepsilon^{*}_{kl}(c) = \alpha_{kl}(c)\Delta T, \tag{A.43}$$

which, together with eqn (A.39) explains the form of the diffusion equation shown in eqn (2.38).

Experiments on solder materials indicate that the stress fields have an observable influence on diffusion. However, if the influence on stresses is described in terms of eqns (A.42) extremely high stresses are necessary to simulate this influence. In an upcoming publication by the authors it is intended to also consider the influence of deformation gradients.